

86805: Software Architectures for Robotics

Localization system for a wheeled humanoid robot

Date: Wed 23:55, 01.02.16

Prof. F. Mastrogiovanni, PhD C. Recchiuto

Rabbia Asghar, BEng, Ernest Skrzypczyk, BSc

Contents

Rollo - Humanoid robot	4
Odometry	4
Clockwise direction	4
Counterclockwise direction	6
Straight line motion	7
Final set of equations	7
Adaptation of odometry model for Rollo	7
Odometry errors	8
Measuring odometry errors	10
System and measurements model	12
System model	12
System model with noise	12
Measurement model with noise	14
Kalman filter	16
Kalman filter equations for linear system	17
Kalman filter equations for non-linear system	17
Extended Kalman filter equations for odometry	18
Practical implementation of extended Kalman filter	19
Divergence of state covariance matrix $\Sigma_{k k}$	20
Robot Operating System (ROS)	21
Mechanical and electrical improvements	25
Simulation and testing	33
Simulation of extended Kalman filter	33
Testing of extended Kalman filter	33
Conclusions	44

List of Figures

1	Odometry model with the simplified 2 wheel configuration for the right turn.	5
2	Odometry model with the simplified 4 wheel configuration for the left turn.	5
3	Odometry model derivation using trigonometry for computation of position and orientation during movement.	6
4	Basic structure of developed ROS nodes.	22
5	Rollo at initial state of project.	25
6	Wires and connectors of Rollo.	26
7	Wooden stabilization pieces after cutting and drilling holes used to make the Rollo more rigid.	26
8	Rollo disassembled.	27
9	Lower legs of Rollo.	27
10	Preparation of power connectors for the microcontroller boards with help of thermoshrink.	28
11	Power connector in final state.	28
12	Voltage regulator with new power cables. The cable tie was used to secure the damaged power connector case, which was of very poor quality.	29
13	Control cable for the motor controller with a connector table for easy access.	29
14	Motor controller using proper control signal connectors with high quality isolation and new power cables.	30
15	Power and control signal cables secured using cable ties. The encoders were connected using professional soldering technique and isolated properly.	30
16	Encoder and motor controller connections to the microcontroller board using IDE40 cables.	31
17	Final state of Rollo after improvements. Additional hardware in form of Kinect andd RaspberryPi have been added for another project.	32
18	Results of EKF simulation based on a log file.	33
19	Results of EKF simulation based on a log file for longer iterations to verify stability.	34
20	Real time visualization: localization of the robot based on EKF, odometry alone and the measurement.	36
21	Test 1, velocity command 19% for both left and right wheels, $q = 0.1, r = 0.1$	36
22	Test 1, velocity command 19% for both left and right wheels, $q = 0.1, r = 0.1$. Figure shows all three states with respect to time.	37
23	Test 2, velocity command 12% for both left and right wheels, $q = 0.1, r = 1.0$	38
24	Test 2, velocity command 12% for both left and right wheels, $q = 0.1, r = 1.0$. Figure shows all three states with respect to time.	38
25	Test 3, velocity command 12% for left wheel and 19% for right wheel, $q = 0.1, r = 10$	39
26	Test 3, velocity command 12% for left wheel and 19% for right wheel, $q = 0.1, r = 10$. Figure shows all three states with respect to time.	39
27	Test 4, velocity command 19% for left wheel and 12% for right wheel, $q = 1.0, r = 10$	40
28	Test 4, velocity command 19% for left wheel and 12% for right wheel, $q = 1.0, r = 10$. Figure shows all three states with respect to time.	40
29	Test 5, velocity command 12% for left wheel and 19% for right wheel, $q = 10, r = 10$	41

30	Test 5, velocity command 12% for left wheel and 19% for right wheel, $q = 10, r = 10$. Figure shows all three states with respect to time.	41
31	Test 6, velocity command 19% for left wheel and 12% for right wheel, $q = 100, r = 10$	42
32	Test 6, velocity command 19% for left wheel and 12% for right wheel, $q = 100, r = 10$. Figure shows all three states with respect to time.	42
33	Test 7, velocity command 12% for left wheel and 19% for right wheel, $q = 8, r = 32$	43
34	Test 8, velocity command 12% for left wheel and 19% for right wheel, $q = 8, r = 32$. Figure shows all three states with respect to time.	43

Rollo - Humanoid robot

Odometry

Odometry is one of the most widely used technique for determining the position of a mobile robot^{1 2}. It mainly involves use of various encoders, for example on wheels, as sensors to estimate the robot's position relative to a starting or previous location. Usually, it is used for real-time positioning in the between the periodic absolute position measurements, for example GPS (Global Positioning System) provides absolute position feedback, however it updates at $0.1 \div 1\text{s}$ interval, during which odometry could be used for localization. One of the major downsides of odometry is its sensitivity to errors. There are various error sources discussed in section Odometry errors on page 8 in detail. One significant source of error influencing the accuracy of odometry that is worth mentioning however, is the integration of velocity measurements over time to give position estimates.

First the odometry based physical motion model for the robot will be derived. The model is derived based on the following important assumptions:

1. The robot is a rigid body
2. The model represents a differential drive robot
3. The wheels of the robot are perfect discs and have the same diameters
4. The wheels have no thickness
5. There is no slip in the wheels
6. Both wheels are turning in the forward direction

A differential drive robot runs straight when the linear speed of both the left and right wheel is same. If the speed of one wheel is greater than the other, the robot runs in an arc. This derivation can be divided in three distinct cases of robot motion:

1. Clockwise direction
2. Counterclockwise direction
3. Straight line

The basic premise for the odometry model of the Rollo humanoid robot is presented in figures 1 and 2.

Clockwise direction

First the case is considered, when the speed of left wheel is greater than the right and the robot will run in clockwise direction. Both right and left wheel will rotate around the same center of a circle.

P_i represents the initial position of the robot defined by the center of the line joining two wheels, while l represents wheel base, ergo distance between or axle length of two wheels. S_L and S_R represent the distance travelled by left and right wheel respectively. $\Delta\Theta$ represents the angle of travel for both the wheels and r is the radius of travel from the center of robot. With encoder feedback from left and right wheel, S_L and S_R can simply be computed using equations (1) and (2)

$$S_L = \frac{n_L}{60} 2\pi r_L t \quad (1)$$

¹ UMBmark – A Method for Measuring, Comparing, and Correcting Odometry Errors in Mobile Robots

² Comparative Study of Localization Techniques for Mobile Robots based on Indirect Kalman Filter

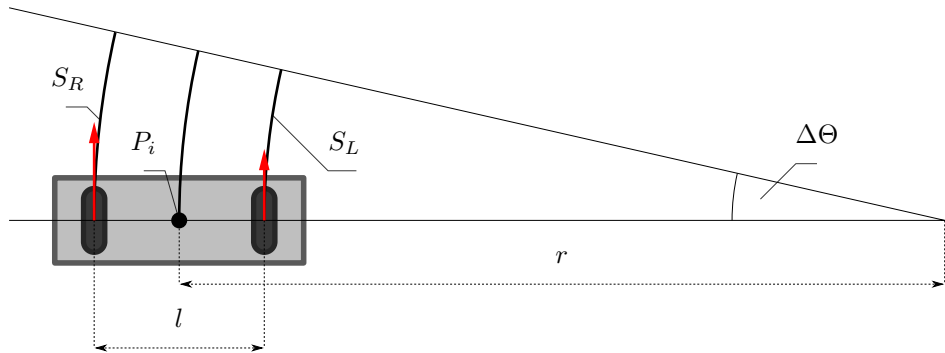


Figure 1: Odometry model with the simplified 2 wheel configuration for the right turn.

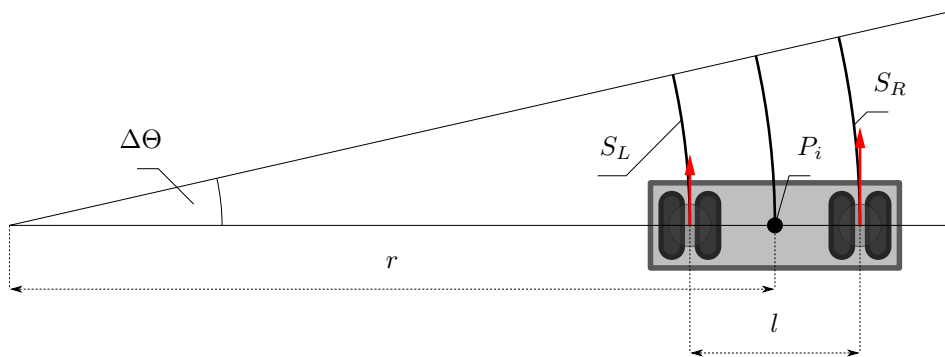


Figure 2: Odometry model with the simplified 4 wheel configuration for the left turn.

$$S_R = \frac{n_R}{60} 2\pi r_R t \quad (2)$$

where n_L and n_R are the revolutions per minute ([rpm]) of left and right wheel, r_L and r_R are the radii of the two wheels and t is time step in seconds.

S_L and S_R can be related to r and $\Delta\Theta$ using formulas (3) and (4)

$$S_L = (r + \frac{l}{2})\Delta\Theta \quad (3)$$

$$S_R = (r - \frac{l}{2})\Delta\Theta \quad (4)$$

The equations (3) and (4) above can be solved simultaneously to compute $\Delta\Theta$ defined in (5).

$$\Delta\Theta = \frac{S_L - S_R}{l} \quad (5)$$

The length between initial position P_i and final position P_f can be approximated by taking average of S_L and S_R .

$$\Delta S = \frac{S_L + S_R}{2} \quad (6)$$

Final position of the robot P_f and its orientation Θ_f can then be derived using basic trigonometry and geometry relations as shown in figure 3 and portrayed in equation (7). In general case the length of arc S

connecting P_i and P_f can be approximated as ΔS . This is because ΔS is very convenient to compute from encoders feedback and the two lengths are almost equal for a very small movements and step of time. This is basically the same technique used to compute π or similar analogue to digital conversion problems. Should the time step increase however, then the error between S and ΔS , represented as red area, will grow, making the approximation very inaccurate.

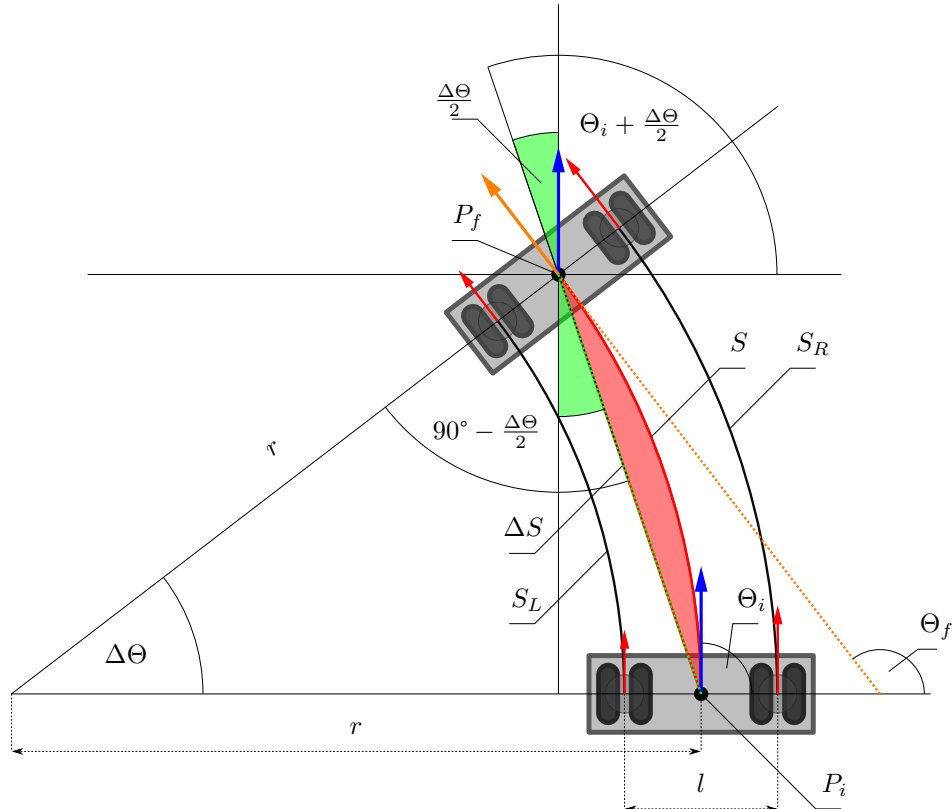


Figure 3: Odometry model derivation using trigonometry for computation of position and orientation during movement.

$$P_f = [P_{ix} + \Delta S(\cos(\Theta_i - \frac{\Delta\Theta}{2})), \quad P_{iy} + \Delta S(\sin(\Theta_i - \frac{\Delta\Theta}{2}))] \quad (7)$$

$$\Theta_f = \Theta_i - \Delta\Theta$$

where Θ_f and Θ_i are the final and initial orientation respectively.

Counterclockwise direction

Similar derivation of the robot can be derived for counterclockwise rotation, when the revolutions per minute of right wheel are higher than that of the left wheel. $\Delta\Theta$ can be computed as shown in (8)

$$\Delta\Theta = \frac{S_R - S_L}{l} \quad (8)$$

The relations for final position and rotation are as follows (9).

$$P_f = \left[P_{ix} + \Delta S(\cos(\Theta_i + \frac{\Delta\Theta}{2})), \quad P_{iy} + \Delta S(\sin(\Theta_i + \frac{\Delta\Theta}{2})) \right] \quad (9)$$

$$\Theta_f = \Theta_i + \Delta\Theta$$

where Θ_f and Θ_i are the final and initial orientation respectively.

Straight line motion

In case of straight line motion, the orientation of the robot stays the same, therefore $\Delta\Theta$ in this case is 0 and S_L is the same as S_R . The relations for final position and rotation are as follows:

$$P_f = [P_{ix} + S_{L=R} \cos(\Theta_i), \quad P_{iy} + S_{L=R} \sin(\Theta_i)] \quad (10)$$

$$\Theta_f = \Theta_i$$

Final set of equations

With the derivation of formulas understood for all three cases, for the ease of computation it is desirable to have the same set of equations in all cases.

The equations selected for this model are as follows.

$$\Delta\Theta = \frac{S_L - S_R}{l} \quad (11)$$

$$\Delta S = \frac{S_L + S_R}{2} \quad (12)$$

$$P_f = \left[P_{ix} + \Delta S(\cos(\Theta_i - \frac{\Delta\Theta}{2})), \quad P_{iy} + \Delta S(\sin(\Theta_i - \frac{\Delta\Theta}{2})) \right] \quad (13)$$

$$\Theta_f = \Theta_i - \Delta\Theta$$

The standalone Python script `rollo_compute_position.py` can provide further details on the odometry model.

Adaptation of odometry model for Rollo

During the project realization the encoders feedback was unavailable in the robot and a physical odometry model could not have been implemented. However, an attempt has been made to implement its modified version. In absence of encoders feedback, the distance covered by left and right wheels is instead estimated from the control command.

In order to implement this simplification initial tests were conducted with Rollo. The robot was run in a straight line, constant curvature arcs and performed rotations at different commands. Rollo's location feedback from the motion capture system was logged. For a given command, average speed of left and right wheel was determined from the recorded data. Matlab environment was used to perform analysis of logged data according to following algorithm:

1. The position in x and y coordinates of Rollo was plotted along with *line of best fit* for the data set.
2. For the displacement of the robot total distance travelled by the robot and change in orientation was determined using the *line of best fit*.
3. Using the timestamps from the recorded data, distance travelled and change in orientation were determined for a unit of time.
4. The rotation speeds of the wheels were determined using the relation in equations (1) \div (6).

The above procedure is based on the assumption that there was no linear acceleration at a given velocity command and the rate of change of robot's orientation was constant.

For simplicity only the forward motion was modelled.

Table 1 shows the predetermined angular velocities of the wheel for given command velocities determined according to the on the preceding page algorithm.

Table 1: Predetermined wheels angular velocity based on test logs for given forward command.

Velocity command		Angular velocity	
Left v_L [%]	Right v_R [%]	Left n_L [rad/s]	Right n_R [rad/s]
6	6	1.381	1.382
12	12	9.530	9.531
19	19	16.729	16.736
56	56	32.040	31.250
12	19	11.778	11.998
19	12	11.978	11.720
31	38	27.974	28.113
31	31	23.798	23.684

Challenges in the modelling of Rollo

1. Due to the mechanical differences in the two legs of Rollo, it is almost impossible for the two wheels to run at the same speed. Moreover, the two motors are powered using two different battery packs and are run in open loop. The difference in voltage level of battery packs results in a different current at the same velocity command using pulse-width modulation increasing the overall velocity error.
2. The robot randomly skids and changes its orientation even for a straight line run. This is partly due to mechanical properties of the robot, partly due to the surface of the laboratory, which serves as testing area and is uneven. The rubber of the tyres lacks sufficient grip on the floor to prevent skidding. One of the Rollo's wheels is visibly skewed. This is a major source for deviation in behaviour of robot's adjusted odometry model.
3. The odometry model is based on the assumption that the wheels have no thickness and have only one point of contact with ground surface. Rollo has four powered wheels by two motors, where each wheel is a 4cm thick. Additionally there are four support wheels in front and back of the two major wheel sets, so that Rollo does not fall over.

Odometry errors

As briefly discussed above, odometry is very sensitive to errors. However, results of odometry based models can be improved by rapid and accurate data collection, equipment calibration and processing of acquired data.

The sources of odometry errors can be broadly divided into two categories:

1. Systematic errors
2. Non-systematic errors

Systematic errors

Systematic errors are caused by inherent properties of the system. They are usually the result of imperfections in the design, production and mechanical construction of a mobile robot and its components. In ideal environment conditions, like most smooth indoor surfaces, systematic errors play a much bigger role than non-systematic errors. Systematic errors also accumulate constantly over time.

In general case there are three main sources of systematic errors in odometry of wheeled robots during a robot's movement:

- Distance
- Rotation
- Skew

Distance error accumulates with the robot travelling. Rotation and skew errors are of less significance with small distance and speed movements, however they are usually dominant with time and influence the overall error more than the distance error.

The major sources of the systematic error in an odometry model of a wheeled robot from a mechanical point of view are unequal diameters of wheels and the uncertainty about the effective wheelbase. Rollo consists of four plastic tyres covered in rubber stripes, two wheels on each side with additional four supporting wheels preventing Rollo from falling over.

Rubber on tyres helps improve traction, however with time rubber compresses differently under asymmetric load distribution. The diameters of wheels are used in computing S_L and S_R as shown in equations (1) and (2).

Furthermore, the contact area between the wheels of Rollo and the floor is comparatively wide for a robot of its size. This introduces difficulties in determining the wheelbase of the robot. Wheelbase is used in computation of angle of travel $\Delta\Theta$ as shown in equation (11).

Other examples of sources of mechanical errors include:

- Average of both wheel diameters differ from nominal diameter
- Misalignment of wheels
- Unbalanced wheels
- Digitalization of acquired data (encoder sampling rate and digital to analog converter resolution)

Non-systematic errors

Non-systematic errors are caused by unknown or unpredictable changes in the system and in the environmental conditions. In wheeled mobile robots, they are usually caused by uneven floors, like in the case of testing area of Rollo. On rough surfaces with significant irregularities, non-systematic errors may be more dominant over systematic errors. On contrary to systematic errors, non-systematic errors do not accumulate with time, but occur randomly.

Possible examples of non-systematic errors are:

- Travel over uneven floors or unexpected objects on the floor
- Wheelslip due to:

- Slippery floors
- Over-acceleration
- Fast turning (skidding)
- Temporal loss of wheel contact with the floor

Measuring odometry errors

University of Michigan Benchmark test (UMBmark) procedure was supposed to be used to determine odometry errors and calibrate the provided system. This procedure was developed by Johann Borenstein and Liqiang Feng around 1995 at the University of Michigan's Advanced Technologies Laboratories. Further details of the test can be found in the research paper UMBmark: A Benchmark Test for Measuring Odometry Errors in Mobile Robots.

As discussed in Systematic errors on the previous page, there are two dominant sources of systematic errors in odometry: unequal wheel diameters and the uncertainty about the effective wheelbase.

Unfortunately, due to unavailability of encoder feedback estimations of S_L and S_R are done using the command given to the robot, so the control input. This means, that equations (1) and (2) are not used in the modified model.

Even if it should be possible to determine the error in the relative size of the wheels and the error due to the uncertainty in effective wheelbase, those can not be corrected or calibrated in the current model. However, the details of the procedure to determine effective wheelbase are described in this section.

As can be seen in the equation (11), incorrect wheelbase value will introduce a significant error in computation of angle of travel $\Delta\Theta$. This error E_b , is directly proportional to the effective wheelbase in relation to the nominal wheelbase l :

$$E_b = \frac{\text{effective wheelbase}}{l} \quad (14)$$

After computing error E_b , the nominal wheelbase in equation (11) can be replaced by effective wheelbase. Thus, this error can be corrected by multiplying the nominal wheelbase b_n with the error factor E_b resulting in the effective wheelbase b_e :

$$\Delta\Theta = \frac{S_L - S_R}{E_b \cdot l} \quad (15)$$

The error E_b can be determined using UMBmark square test procedure, whose summary for Rollo is as follows:

1. At the beginning of or before the actual run, measurements of the absolute position and orientation of Rollo using motion capture system are performed along with initialization of vehicle's odometry program to the starting point.
2. Running the vehicle through a $2 \times 2 m$ square path in clockwise direction while making sure to:
 - (a) stop after each $2 m$ straight segment,
 - (b) make a total of four 90° -turns on the spot,
 - (c) run the vehicle slowly to avoid slippage.
3. After returning to the starting area, again measurements of the absolute position and orientation of Rollo are performed using motion capture system.
4. Comparing between the absolute position and robot's calculated position using equations (16), (17) and (18).

$$\epsilon x = x_{abs} - x_{calc} \quad (16)$$

$$\epsilon y = y_{abs} - y_{calc} \quad (17)$$

$$\epsilon \theta = \theta_{abs} - \theta_{calc} \quad (18)$$

$\epsilon x, \epsilon y, \epsilon \theta$ – Position and orientation errors due to odometry model

$x_{abs}, y_{abs}, \theta_{abs}$ – Absolute position and orientation of Rollo

$x_{calc}, y_{calc}, \theta_{calc}$ – Calculated position and orientation of Rollo using odometry model

5. Repetition of steps 1 ÷ 4 for four more times, giving a total of five runs.
6. Repetition of steps 1 ÷ 5 in counterclockwise direction.
7. Computation of center of gravity coordinates for each cluster in clockwise and counterclockwise directions using equations (19) and (20), where n is the number of runs, so $n = 5$ in the proposed scenario.

$$x_{cg,cw/ccw} = \frac{1}{n} \sum_{i=1}^n \epsilon x_{i,cw/ccw} \quad (19)$$

$$y_{cg,cw/ccw} = \frac{1}{n} \sum_{i=1}^n \epsilon y_{i,cw/ccw} \quad (20)$$

8. Computation of E_b using equations (21),(22) and (23)

$$E_b = \frac{90^\circ}{90^\circ - \alpha} \quad (21)$$

where α can be defined as

$$\alpha = \frac{x_{cg,cw} + x_{cg,ccw}}{-4L} \frac{180^\circ}{\pi} \quad (22)$$

or

$$\alpha = \frac{y_{cg,cw} - y_{cg,ccw}}{-4L} \frac{180^\circ}{\pi} \quad (23)$$

and L represents the side of square segment, for the given test area conditions in case of Rollo $L = 2 m$.

System and measurements model

System model

In order to implement Kalman filter³, the previously described model must be first represented in state space. Location of the robot can be defined at instant k using state variables (24), which include position in x and y coordinates and orientation Θ .

$$x_k = \begin{bmatrix} x_{[x],k} \\ x_{[y],k} \\ x_{[\theta],k} \end{bmatrix} \quad (24)$$

The control input provided to robot consists of left and right wheel speeds. This defines the distance covered by both the wheels in a given unit of time. The relative displacement of the robot at instant k can be notated by d_k . Using equations (7), (9) and (10), derived on page 6, relative displacement can be expressed in terms of ΔS and $\Delta\Theta$. Thus, control input u_k can be expressed as a function of relative displacement d_k .

$$u_k = j(d_k) \quad (25)$$

$$u_k = \begin{bmatrix} u_{[\Delta S],k} \\ u_{[\Delta \theta],k} \end{bmatrix}$$

Given x_{k-1} and u_{k-1} , the next location of the robot x_k can be computed.

$$x_k = f(x_{k-1}, u_{k-1}) = \begin{bmatrix} f_x(x_{k-1}, u_{k-1}) \\ f_y(x_{k-1}, u_{k-1}) \\ f_\theta(x_{k-1}, u_{k-1}) \end{bmatrix} \quad (26)$$

In the above derivation of the system model it was assumed that there are no noise sources. In the next section, noise has been modelled into the system.

System model with noise

First, noise was added to the relative displacement with the assumption, that it can be modelled by a random noise vector q_k such that, the noise is a Gaussian distribution with zero mean \hat{q}_k and covariance matrix U_k .

$$q_k \sim N(\hat{q}_k, U_k) \quad (27)$$

where

$$\hat{q}_k = \begin{bmatrix} 0 \\ 0 \end{bmatrix}$$

and

$$U_k = E(q_k - \hat{q}_k)(q_k - \hat{q}_k)^T$$

³ Rudy Negeborn - Robot Localization and Kalman Filters

$$U_k = \begin{bmatrix} \sigma_{q[\Delta S],k}^2 & \sigma_{q[\Delta \theta],k} \sigma_{q[\Delta S],k} \\ \sigma_{q[\Delta \theta],k} \sigma_{q[\Delta S],k} & \sigma_{q[\Delta \theta],k}^2 \end{bmatrix}$$

With the assumption that the noise sources are independent, the off-diagonal elements of the covariance matrix U_k are equal to zero.

The control input, or relative displacement, can be expressed as shown in (28).

$$u_k = j(d_k) + q_k \quad (28)$$

$$u_k = \begin{bmatrix} u_{[\Delta S],k} \\ u_{[\Delta \theta],k} \end{bmatrix} + \begin{bmatrix} q_{[\Delta S],k} \\ q_{[\Delta \theta],k} \end{bmatrix}$$

This makes u_k a random vector. Assuming, that $u_{[\Delta S],k}$ and $u_{[\theta],k}$ are deterministic, uncertainty in u_k equals the uncertainty in the noise term q_k .

The system noise can similarly be modelled by a random noise vector w_k such that, the noise is a Gaussian distribution with zero mean \hat{w}_k and covariance matrix Q_k . This noise source is not directly related to the relative displacement, however it is inherent to the system. Modelling errors, odometry errors, discretization and approximations involved in the derivation of the model all play a part in this noise source. Noise vector w_k is represented in equation (29).

$$w_k \sim N(\hat{w}_k, Q_k) \quad (29)$$

where

$$\hat{w}_k = \begin{bmatrix} 0 \\ 0 \\ 0 \end{bmatrix}$$

and

$$Q_k = E(w_k - \hat{w}_k)(w_k - \hat{w}_k)^T$$

$$Q_k = \begin{bmatrix} \sigma_{w[x],k}^2 & \sigma_{w[y],k} \sigma_{w[x],k} & \sigma_{w[\theta],k} \sigma_{w[x],k} \\ \sigma_{w[x],k} \sigma_{w[y],k} & \sigma_{w[y],k}^2 & \sigma_{w[\theta],k} \sigma_{w[y],k} \\ \sigma_{w[x],k} \sigma_{w[\theta],k} & \sigma_{w[y],k} \sigma_{w[\theta],k} & \sigma_{w[\theta],k}^2 \end{bmatrix}$$

With the assumption that the noise sources are independent, the off-diagonal elements of the covariance matrix Q_k are presumably zero. Determination of matrix Q_k is discussed in section Practical implementation of extended Kalman filter on page 19.

The system can be expressed as shown below.

$$x_k = f(x_{k-1}, u_{k-1}) + w_k \quad (30)$$

$$x_k = \begin{bmatrix} f_x(x_{k-1}, u_{k-1}) \\ f_y(x_{k-1}, u_{k-1}) \\ f_\theta(x_{k-1}, u_{k-1}) \end{bmatrix} + \begin{bmatrix} w_{[x], k-1} \\ w_{[y], k-1} \\ w_{[\theta], k-1} \end{bmatrix} \quad (31)$$

x_k is a random vector and with every time step the variance of system noise increases. Therefore the variance of the location grows with every time step also.

The proposed system model was prepared for the implementation of Kalman filter, which requires as next step the preparation of the measurement model.

Measurement model with noise

Starting with the assumption that there is no noise in the measurement, measurement vector z_k simply consists of the corresponding state variables and is defined by equation (32).

$$z_k = \begin{bmatrix} z_{[x], k} \\ z_{[y], k} \\ z_{[\theta], k} \end{bmatrix} \quad (32)$$

In the proposed system, motion capture system available in the laboratory is used to localize Rollo. It acts as absolute sensor by providing directly the position in x and y coordinates and orientation θ of the robot. Thus, z_k in this case is simply expressed as (33).

$$z_k = \begin{bmatrix} x_{[x], k} \\ x_{[y], k} \\ x_{[\theta], k} \end{bmatrix} \quad (33)$$

Provided that the motion capture system is not noise free, this has been incorporated into the measurement model. With the assumption, that measurement noise can be modelled by a random noise vector v_k such that, the noise is a Gaussian distribution with zero mean \hat{v}_k and covariance matrix R_k .

$$v_k \sim N(\hat{v}_k, R_k) \quad (34)$$

where

$$\hat{v}_k = \begin{bmatrix} 0 \\ 0 \\ 0 \end{bmatrix}$$

and

$$R_k = E(v_k - \hat{v}_k)(v_k - \hat{v}_k)^T$$

$$R_k = \begin{bmatrix} \sigma_{v[x], k}^2 & \sigma_{v[y], k} \sigma_{v[x], k} & \sigma_{v[\theta], k} \sigma_{v[x], k} \\ \sigma_{v[x], k} \sigma_{v[y], k} & \sigma_{v[y], k}^2 & \sigma_{v[\theta], k} \sigma_{v[y], k} \\ \sigma_{v[x], k} \sigma_{v[\theta], k} & \sigma_{v[y], k} \sigma_{v[\theta], k} & \sigma_{v[\theta], k}^2 \end{bmatrix}$$

Again, assuming that the noise sources are independent, the off-diagonal elements of the covariance matrix R_k are presumably zero.

The final measurement model can be expressed as shown in (36).

$$z_k = x_k + v_k \quad (35)$$

$$z_k = \begin{bmatrix} x_{[x],k} \\ x_{[y],k} \\ x_{[\theta],k} \end{bmatrix} + \begin{bmatrix} v_{[x],k-1} \\ v_{[y],k-1} \\ v_{[\theta],k-1} \end{bmatrix} \quad (36)$$

Since the measurement noise v_k is a Gaussian random vector, this makes z_k a random vector.

Kalman filter

Kalman filter is an algorithm that uses a series of measurements observed over time, containing statistical noise and other inaccuracies, and produces estimates of unknown variables that tend to be more precise than those based on a single measurement alone⁴.

A physical system is driven by a set of external inputs or controls. Its outputs are evaluated by sensors such that, the knowledge on the system's behaviour is solely given by the inputs and the observed outputs. For example, in case of Rollo, the physical system is a mobile robot and given is the problem of localizing it. The control, or the input, is defined by the velocity command given to the left and right wheels, which determines the relative displacement of Rollo. The observed output is the position and orientation of Rollo measured from the motion capture system. The observations convey the errors and uncertainties in the process, namely the sensor noise and the system errors. Based on the available information (control inputs and observations), Kalman filter computes an estimate of the system's state by minimizing the variance of the estimation error. From a theoretical standpoint, the main assumptions of the Kalman filter are that the underlying system is a linear dynamical system and that all error terms and measurements have a Gaussian distribution.

Kalman filtering is a recursive analytical technique involving two main steps: prediction and innovation.

Prediction is also known as *time update* and refers to prediction of state variables using information from previous state and control input. This step does not involve using measurement.

Innovation which is also known as *correction* or *measurement update* refers to estimation of state variable using measurement.

Kalman filter is broadly used in robotics for solving the localization problem, because of its efficiency and accuracy. Some of its characteristics are:

1. Very easy implementation
2. Computationally efficient, updates filter when providing new measurements to the existing data set
3. Uncertainty estimates are provided as part of the filter
4. Recursive algorithm, which makes it suitable for real time applications using only the present input measurements and the previously calculated state.

All members of Kalman family of filters like extended Kalman filter and unscented Kalman filter, comply with a structured sequence of six steps per iteration:

1. **State estimate time update:** An updated state prediction $\hat{x}_{k|k-1}$ is made, based on a priori information and the system model.
2. **Error covariance time update:** The second step is to determine the predicted state-estimate error covariance matrix $\Sigma_{k|k-1}$ based on a priori information and the system model.
3. **Estimate system output:** The third step is to estimate the system's output \hat{z}_k corresponding to the timestamp of the most recently received measurement using present a priori information.
4. **Estimator gain matrix:** The fourth step is to compute the estimator gain matrix H_k .
5. **State estimate measurement update:** The fifth step is to compute the a posteriori state estimate $\hat{x}_{k|k}$ by updating the a priori estimate using the estimator gain and the output prediction error.
6. **Error covariance measurement update:** The final step computes the a posteriori error covariance matrix $\Sigma_{k|k}$.

⁴e-Study Guide for: Introduction to Probability Theory and Stochastic Processes

Kalman filter equations for linear system

In order to implement Kalman filter first represent the linear system as follows.

$$\begin{aligned} x_{k+1} &= A_k x_k + B_k u_k + w_k \\ z_k &= C_k x_k + v_k \end{aligned} \quad (37)$$

where $w_k \sim N(0, Q_k)$ and $v_k \sim N(0, R_k)$ as described in System model with noise on page 12 and Measurement model with noise on page 14 respectively.

For Kalman filter A , B , C , Q and R can be time variant. However, for simplicity it is assumed that they are time invariant for the provided system. Given initial state estimate $\hat{x}_{0|0}$ and initial state covariance matrix $\Sigma_{0|0}$ the Kalman filter can be computed using following set of equations.

Prediction (time update)

$$\begin{aligned} \hat{x}_{k|k-1} &= A \hat{x}_{k-1|k-1} + B u_{k-1} \\ \Sigma_{k|k-1} &= A \Sigma_{k-1|k-1} A^T + Q \end{aligned} \quad (38)$$

Innovation (measurement update)

$$\begin{aligned} H_k &= \Sigma_{k|k-1} C^T (C \Sigma_{k|k-1} C^T + R)^{-1} \\ \hat{x}_{k|k} &= \hat{x}_{k|k-1} + H_k [z_k - C \hat{x}_{k|k-1}] \\ \Sigma_{k|k} &= [I - H_k C] \Sigma_{k|k-1} \end{aligned} \quad (39)$$

Kalman filter equations for non-linear system

Now we consider a non-linear extension to the Kalman filter, *Extended Kalman Filter (EKF)*. The EKF implements Kalman filter for non-linear system dynamics that result from the linearization of the original non-linear filter dynamics around the previous state estimates.

A non linear system can be represented as follows.

$$\begin{aligned} x_k &= f(x_{k-1}, u_{k-1}) + w_{k-1} \\ z_k &= h(x_k) + v_{k-1} \end{aligned} \quad (40)$$

where $w_k \sim N(0, Q_k)$ and $v_k \sim N(0, R_k)$.

Another assumption is that $f(\cdot)$, $h(\cdot)$, Q and R are time invariant for the provided non-linear system. $f(\cdot)$ and $h(\cdot)$ are linearized about the prior best estimate of the states at each instant of time by finite difference method in order to compute covariances. Given initial state estimate $\hat{x}_{0|0}$ and initial state covariance matrix $\Sigma_{0|0}$ the extended Kalman filter can be computed using following set of equations.

Prediction (time update)

$$\begin{aligned} \hat{x}_{k|k-1} &= f(\hat{x}_{k-1|k-1}, u_{k-1}) \\ \Sigma_{k|k-1} &= J_f \Sigma_{k-1|k-1} J_f^T + Q \end{aligned} \quad (41)$$

Innovation (measurement update)

$$\begin{aligned} H_k &= \Sigma_{k|k-1} J_h^T (J_h \Sigma_{k|k-1} J_h^T + R)^{-1} \\ \hat{x}_{k|k} &= \hat{x}_{k|k-1} + H_k [z_k - h(\hat{x}_{k|k-1})] \\ \Sigma_{k|k} &= [I - H_k J_h] \Sigma_{k|k-1} \end{aligned} \quad (42)$$

where J_f and J_h are the jacobian matrices.

J_f is the jacobian matrix containing the partial derivative of the system function $f(\cdot)$ with respect to the state x , evaluated at the last state estimate $\hat{x}_{k-1|k-1}$ and control input u_{k-1} .

J_h is the jacobian matrix containing partial derivatives of the measurement function $h(\cdot)$ with respect to the state x , evaluated at the prior state estimate $\hat{x}_{k|k-1}$.

Extended Kalman filter equations for odometry

After deriving physical model of the provided system for Odometry and understanding the extended Kalman filter in Kalman filter equations for non-linear system, preparation for the EKF equations for odometry can be done.

$$\begin{bmatrix} x_{[x],k} \\ x_{[y],k} \\ x_{[\theta],k} \end{bmatrix} = \begin{bmatrix} f_x(x_{k-1}, u_{k-1}) \\ f_y(x_{k-1}, u_{k-1}) \\ f_\theta(x_{k-1}, u_{k-1}) \end{bmatrix} + \begin{bmatrix} w_{[x],k-1} \\ w_{[y],k-1} \\ w_{[\theta],k-1} \end{bmatrix} \quad (43)$$

$$\begin{bmatrix} x_{[x],k} \\ x_{[y],k} \\ x_{[\theta],k} \end{bmatrix} = \begin{bmatrix} x_{[x],k-1} + u_{[\Delta]S,k-1} \cdot \cos(x_{[\Theta],k-1} - \frac{u_{[\Delta\Theta],k-1}}{2}) \\ x_{[y],k-1} + u_{[\Delta]S,k-1} \cdot \sin(x_{[\Theta],k-1} - \frac{u_{[\Delta\Theta],k-1}}{2}) \\ x_{[\theta],k-1} - u_{[\Delta\Theta],k-1} \end{bmatrix} + \begin{bmatrix} w_{[x],k-1} \\ w_{[y],k-1} \\ w_{[\theta],k-1} \end{bmatrix} \quad (44)$$

Prediction (time update)

$$\begin{bmatrix} \hat{x}_{[x],k|k-1} \\ \hat{x}_{[y],k|k-1} \\ \hat{x}_{[\theta],k|k-1} \end{bmatrix} = \begin{bmatrix} \hat{x}_{[x],k-1|k-1} + u_{[\Delta]S,k-1} \cdot \cos(\hat{x}_{[\Theta],k-1|k-1} - \frac{u_{[\Delta\Theta],k-1}}{2}) \\ \hat{x}_{[y],k-1|k-1} + u_{[\Delta]S,k-1} \cdot \sin(\hat{x}_{[\Theta],k-1|k-1} - \frac{u_{[\Delta\Theta],k-1}}{2}) \\ \hat{x}_{[\theta],k-1|k-1} - u_{[\Delta\Theta],k-1} \end{bmatrix} \quad (45)$$

$$\begin{aligned} J_{f,k} &= \frac{\partial f(x)}{\partial x} \Big|_{x=\hat{x}_{k-1|k-1}, u=u_{k-1}} \\ &= \begin{bmatrix} \frac{\partial f_x}{\partial x_{[x]}} & \frac{\partial f_x}{\partial x_{[y]}} & \frac{\partial f_x}{\partial x_{[\theta]}} \\ \frac{\partial f_y}{\partial x_{[x]}} & \frac{\partial f_y}{\partial x_{[y]}} & \frac{\partial f_y}{\partial x_{[\theta]}} \\ \frac{\partial f_\theta}{\partial x_{[x]}} & \frac{\partial f_\theta}{\partial x_{[y]}} & \frac{\partial f_\theta}{\partial x_{[\theta]}} \end{bmatrix} \Big|_{x=\hat{x}_{k-1|k-1}, u=u_{k-1}} \\ &= \begin{bmatrix} 1 & 0 & -u_{[\Delta]S} \cdot \sin(x_{[\Theta]} - \frac{u_{[\Delta\Theta]}}{2}) \\ 0 & 1 & +u_{[\Delta]S} \cdot \cos(x_{[\Theta]} - \frac{u_{[\Delta\Theta]}}{2}) \\ 0 & 0 & 1 \end{bmatrix} \Big|_{x=\hat{x}_{k-1|k-1}, u=u_{k-1}} \end{aligned} \quad (46)$$

$$\Sigma_{[x],k|k-1} = J_f \Sigma_{[x],k-1|k-1} J_f^T + Q \quad (47)$$

Innovation (measurement update)

$$\begin{aligned}
 J_{h,k} &= \frac{\partial h(x)}{\partial x} \Big|_{x=\hat{x}_{k|k-1}} \\
 &= \begin{bmatrix} \frac{\partial h_x}{\partial x_{[x]}} & \frac{\partial h_x}{\partial x_{[y]}} & \frac{\partial h_x}{\partial x_{[\theta]}} \\ \frac{\partial h_y}{\partial x_{[x]}} & \frac{\partial h_y}{\partial x_{[y]}} & \frac{\partial h_y}{\partial x_{[\theta]}} \\ \frac{\partial h_\theta}{\partial x_{[x]}} & \frac{\partial h_\theta}{\partial x_{[y]}} & \frac{\partial h_\theta}{\partial x_{[\theta]}} \end{bmatrix} \Big|_{x=\hat{x}_{k|k-1}, u=u_{k-1}} \\
 &= \begin{bmatrix} 1 & 0 & 0 \\ 0 & 1 & 0 \\ 0 & 0 & 1 \end{bmatrix} \Big|_{x=\hat{x}_{k|k-1}, u=u_{k-1}}
 \end{aligned} \tag{48}$$

Using the above derived jacobian matrix (48) for computation of Kalman gain matrix H_k , a posteriori state estimate and a posteriori error covariance matrix following concludes.

$$\begin{aligned}
 H_k &= \Sigma_{k|k-1} (\Sigma_{k|k-1} + R)^{-1} \\
 \hat{x}_{k|k} &= \hat{x}_{k|k-1} + H_k [z_k - \hat{x}_{k|k-1}] \\
 \Sigma_{k|k} &= [I - H_k J_h] \Sigma_{k|k-1}
 \end{aligned} \tag{49}$$

Practical implementation of extended Kalman filter

Proceeding with the EKF model for odometry, initialization of the model is necessary before practical implementation, which requires following components to be initialized:

1. Initial state estimate $\hat{x}_{0|0}$,
2. Initial state covariance matrix $\Sigma_{0|0}$,
3. Process covariance matrix Q ,
4. Measurement covariance matrix R .

Initial state estimate $\hat{x}_{0|0}$

This is the initial estimate of the state vector required for the first iteration of the EKF. In the provided system, Optitrack Motion Capture system is used for measurement. Optitrack provides ground truth and positional accuracy of up to sub-millimeter range. For performed tests the measurement sensor readings were used to determine $\hat{x}_{0|0}$.

Initial state covariance matrix $\Sigma_{0|0}$

Initial state covariance matrix is based on the initialization error of the state. If the initial state estimate is very close to the actual state, this matrix will contain very small values. With the assumption that noise sources for different state elements are independent, the off diagonal elements of the covariance matrix can be assumed to equal zero.

Usually if this matrix is unknown identity matrix is used, since state covariance matrix is updated in every iteration of EKF. For a stable EKF this matrix should be converging over time. An initial estimate closer to the actual state will offer faster convergence of the Kalman filter.

Since the initial state is determined from the motion capture system, initial state covariance matrix could be assumed to be zero. However, since the chosen procedure simulates a sensor not as accurate as motion capture, the initial state covariance matrix is taken as identity.

Process covariance matrix \mathbf{Q}

This is the error covariance matrix of the process and gives an estimate of uncertainty in the state equations. The uncertainty in the process could be a result of various sources of error, including modeling errors, odometry errors, discretization and approximations involved in the derivation of the model.

In order to get a better understanding of error in the model, computation of error based on odometry model from log files and analysis were performed.

For testing a different range of values for Q was chosen in order to understand the behaviour of the EKF better.

Measurement covariance matrix R

This is the error covariance matrix of measurement sensor and provides a measure of how uncertain the measurement is. As discussed earlier, Optitrack Motion Capture system is used for measurement and it provides ground truth. For the case when the measurement is very accurate, matrix R will carry very small variances and can be approximated to zero. However, in order to simulate EKF for a system, whose measurement sensor is not as accurate, different range of values for the measurement covariance matrix R was used.

Divergence of state covariance matrix $\Sigma_{k|k}$

Proceeding with initialization of EKF as discussed above, it was observed that the filter behaved well for a specific period of time after initialization. However, after a certain amount of time the state covariance matrix started diverging very fast, resulting in failure of the filter.

It was understood that a possible reason behind this could be lack of input excitation that results in growing values of state covariance matrix and large spread of eigenvalues. In order to solve this issue, different techniques can be used to stabilize estimation and prevent windup of state estimation and covariance matrix.

The issue has been solved by performing Cholesky decomposition in the computation of Kalman gain matrix. Cholesky factorization is a decomposition of a Hermitian, a positive-definite matrix, into the product of a lower triangular matrix, or alternatively an upper triangular matrix, and its conjugate transpose. Cholesky decomposition offers numerical stability to the system, which is the main reason it was chosen.

Implementation was based on the assumption that the state covariance matrix $\Sigma_{k|k}$ is symmetrical. This resulted in acceptable behaviour of the filter, however, it slowed down the performance of EKF. With Cholesky decomposition, the innovation update of EKF can be written as shown in (50)

$$\begin{aligned} U &= \text{CholeskyDecomposition}(J_h \Sigma_{k|k-1} J_h^T + R) \\ \hat{x}_{k|k} &= \hat{x}_{k|k-1} + [\Sigma_{k|k-1} U^{-1}] U^{T-1} [z_k - h(\hat{x}_{k|k-1})] \\ \Sigma_{k|k} &= \Sigma_{k|k-1} - [\Sigma_{k|k-1} U^{-1}] [\Sigma_{k|k-1} U^{-1}]^T \end{aligned} \quad (50)$$

where $\text{CholeskyDecomposition}(X)$ produces an upper triangular matrix U from the diagonal and upper triangle of matrix X , thus satisfying the equation $U^T U = X$.

Robot Operating System (ROS)

Robot Operating System (ROS) is a collection of software frameworks for robot software development, it works as middleware for work with complex robotic problems. ROS uses the publisher-subscriber software architecture model for communication between nodes. The presented problem of localization of a humanoid robot using extended Kalman filter, which has been described in detail in Kalman filter, has been solved using ROS. Five nodes have been developed respecting the aspects of modularity and interchangeability of software:

- Preprocessor node
- Control node
- Communication node
- Extended Kalman filter node
- Visualization node

Each node is supposed to fulfil one specific function, so that the software can be used for different tasks and in different environments. However there are several aspects that have been merged into same nodes, that might be contra-intuitive. Functionalities of the nodes are distributed the following way:

- Preprocessor node:
 1. Filter the raw data from motion capture system
 2. Publish filtered data along with timestamp for modelling of odometry and the measurement in Kalman filter
- Control node:
 1. Translate input from keyboard into linear and angular velocities within unitary limits ($-100\% \div 100\%$)
 2. Publish data as Twist message for further processing
- Communication node:
 - A. Normal operation mode
 - (a) Translate data from control node into a three byte message for Rollo
 - (b) Publish decoded velocities
 - (c) Send commands continuously at a given rate to Rollo
 - (d) Perform emergency procedure if connection to control node is lost
 - B. Square test of n-th order based on the UMBmark test procedure described in detail in Measuring odometry errors
 - (a) Perform a cycle of forward movement and turns to move the robot along a square
 - (b) For higher than first order square test turn around between runs
- Extended Kalman filter node:
 1. Initialize EKF
 2. Preprocessing of acquired data to make comparison of relevant information
 3. Estimate of state using EKF

4. Odometry data calculation
 5. Publish results
- Visualization node:
 1. Visualize data holding position and orientation of robot, from preprocessor and extended Kalman filter, which provides estimates of state and odometry data

Nodes have been written in C++ programming language with the exception of visualization node, which has been written in Python, mainly because of easy access to the powerful Matplotlib library. There has been also a significant amount of testing and prototyping of software done in Matlab and Python, mainly for the odometry model and extended Kalman filter implementation as well as analysis. Additional scripts in Bash shell were also written, mostly for the purpose of easier repetition of tasks. All of the significant files can be found in the GitHub repository established for this project.

The basic software architecture model implemented is publish-subscribe given the architecture ROS uses represented by 4 shows the correlation between individual nodes and environment.

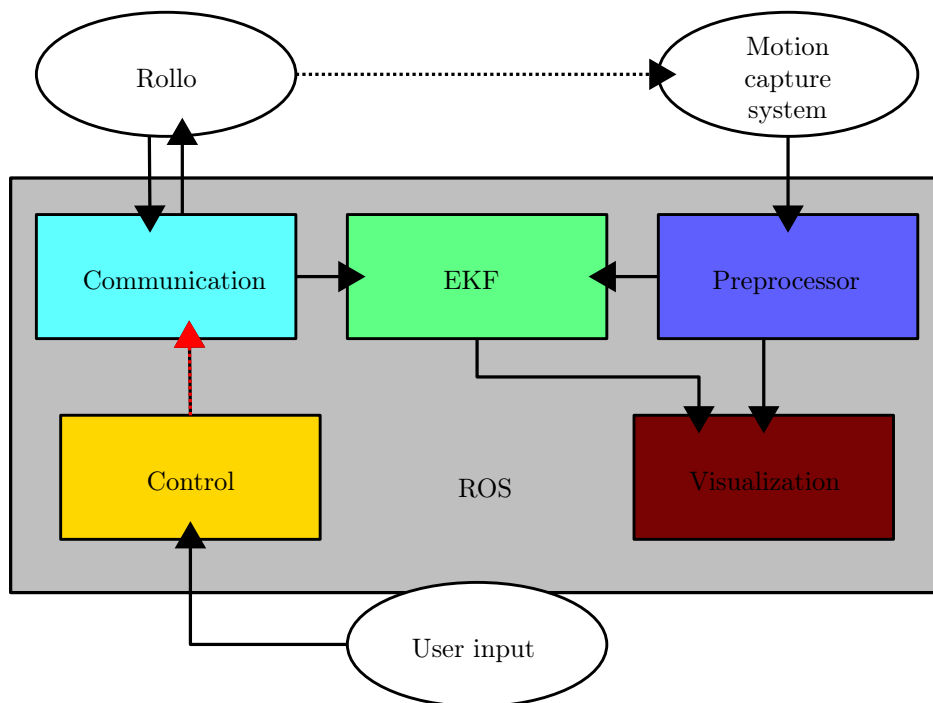


Figure 4: Basic structure of developed ROS nodes.

The Optitrack Motion Capture system and ROS *mocap_optitrack* node are represented as one entity, that receives data through infrared cameras from objects using highly light reflective markers. Rollo recognized by the system, after user input as a rigid body, provides that way it's position and orientation data through the *mocap_optitrack* node. This data gets filtered through the preprocessor node in accordance with user provided parameters, that publishes it with a timestamp. The user provides input in form of keyboard input that the control node interprets and conveys as a standard geometry *Twist* message to the communication node. This node, depending on the operation mode, continuously sends UDP packets to Rollo through provided setup of a wireless router and publishes velocity commands it decoded from the control node to EKF node. The optimal frequency rate for the communication node has been established by trial and error at 10 Hz, where the response to used input is fast enough to stop Rollo without delay. Kalman filter node uses

data from preprocessor and communication node to perform localization of Rollo and publishes estimates of the state. Filtered motion capture data from the preprocessor node and estimates from EKF node as well as the odometry model data act as inputs for the visualization node. This node provides visual feedback of the whole system to the user as shown in figure 20.

Because of the different function each node performs, not every node is necessary to be run, which is clearly visible in the ROS package launcher file `rollo.launch`. It is possible to control rollo only using the control and communication nodes. If connection to the control is lost, depending on user set parameters, the communication node performs the emergency procedure and stays in that mode. This critical aspect has been marked on the graph 4 and is described later in detail. Also the square test can be performed by the communication node alone. The EKF node includes the odometry model. With data provided by the communication node as input EKF node publishes the position and orientation based on the physical odometry model.

A few aspects have been addressed while developing the software. One of those aspects is safety of operation. Should the control node loose connection to the master and at the same time be sending commands other than full stop, where linear and angular velocities are equal to zero, then in normal case the communication node would continue sending data with last values received from control node and the robot would be uncontrollable. This is the reason a safety, or emergency, procedure has been implemented. After a period of time, which can be specified from the command line using the `em` parameter, a full stop command is being send for ten times. Should the control node reestablish connection, the communication node will continue to work in normal procedure.

Since the robot has been tested in laboratory conditions, the algorithm implemented is sufficient for given condition. However it is not very robust and could be further improved. For example, the stop command could be send continuously, until control node is reconnected with ROS master or the communication node forcefully exited. Another improvement would be to send a special message that this event occurred, so that the user is informed about it without delay.

Next feature implemented into the communication node is the square test. This particular test has been implemented in accordance to UMBmark test procedure described in Measuring odometry errors. The implemented algorithm lets the user specify the forward and turning times for the square test, which is necessary in case of not having access to direct odometry data in form of encoder readings. The square test can be performed in multiple runs, so that each cycle includes eight steps of interchanging forward movement and turning.

Should there be multiple runs specified, the robot would turn around after each cycle, which is to rotate 180° and continue with step 1. In other case that would be the last or only run. Ideally the robot would stop at exactly the same position it started with the initial orientation. Since there are systematic and random errors, this is only achievable for a given tolerance. However in case of Rollo, the errors and mechanical structure differences are so great, that the test is basically not practical. During tests runs it has been only confirmed, what the analysis of the logs performed for the extended Kalman filter node concluded, namely that the turning times differ significantly, which is most probably due to mechanical asymmetry.

The square test algorithm has been implemented directly into the communication node, because of easy access to all necessary functions and no conflicts with other nodes. However logically it should either have its own node or be implemented into the control node. However then aspects of priority and safety aspects arise.

Since the encoder feedback from Rollo was unavailable, the communication node did not include necessary code for receiving that data and processing it. Great effort has been undertaken to prepare Rollo from the hardware side for encoder feedback, but in the end the low-level software was missing. This bidirectional communication between Rollo and communication node has been portrayed in diagram 4, since it is a crucial feature for proper implementation of any localization solver.

Further details on the setup and nodes are described in next section Simulation and testing. More in depth documentation of the actual code and algorithms has been done using Doxygen in two formats: HTML

version and local LaTeX document form.

Mechanical and electrical improvements

At the initial stage of the project it became apparent that several changes and improvements needed to be introduced to Rollo in order to complete the assignment. Rollo was developed to simulate human walking motion. The legs consisted of springs, making the whole structure very flexible as shown in figure 5. Also the electrical components were connected in a suboptimal way as portrayed by image in figure 6.

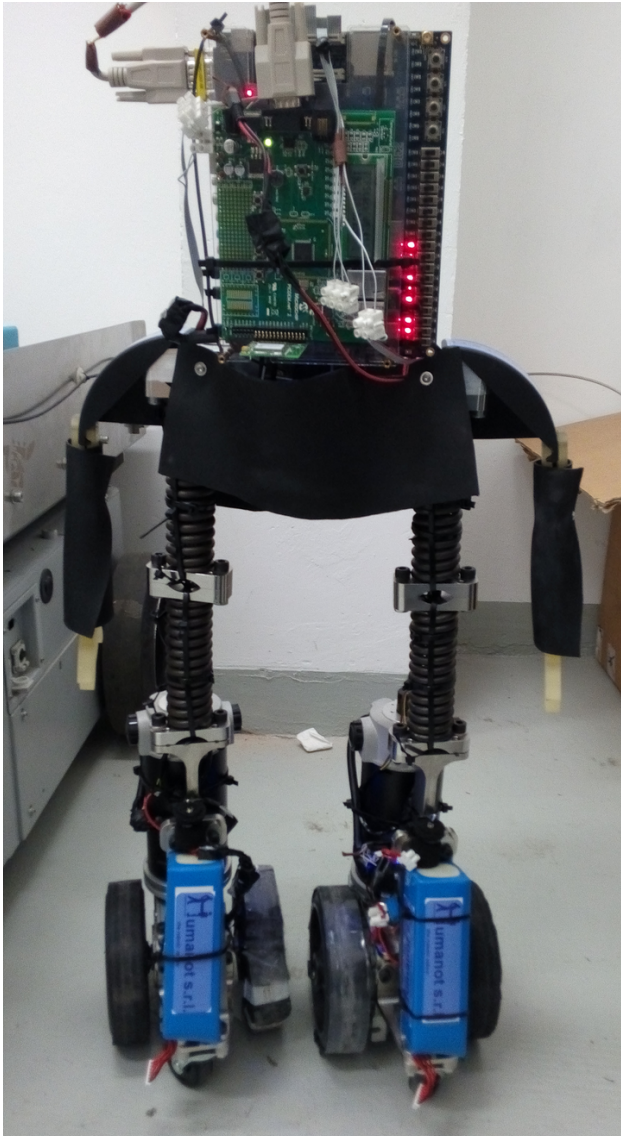


Figure 5: Rollo at initial state of project.

This setup introduced additional errors in the movement and furthermore also localization of Rollo, which is the reason additional wooden structure was implemented to make the robot more rigid and the movements more predictable. The whole process is documented in figures 7 ÷ 9 for the mechanical part and figures 10 ÷ 16 for the electrical part.

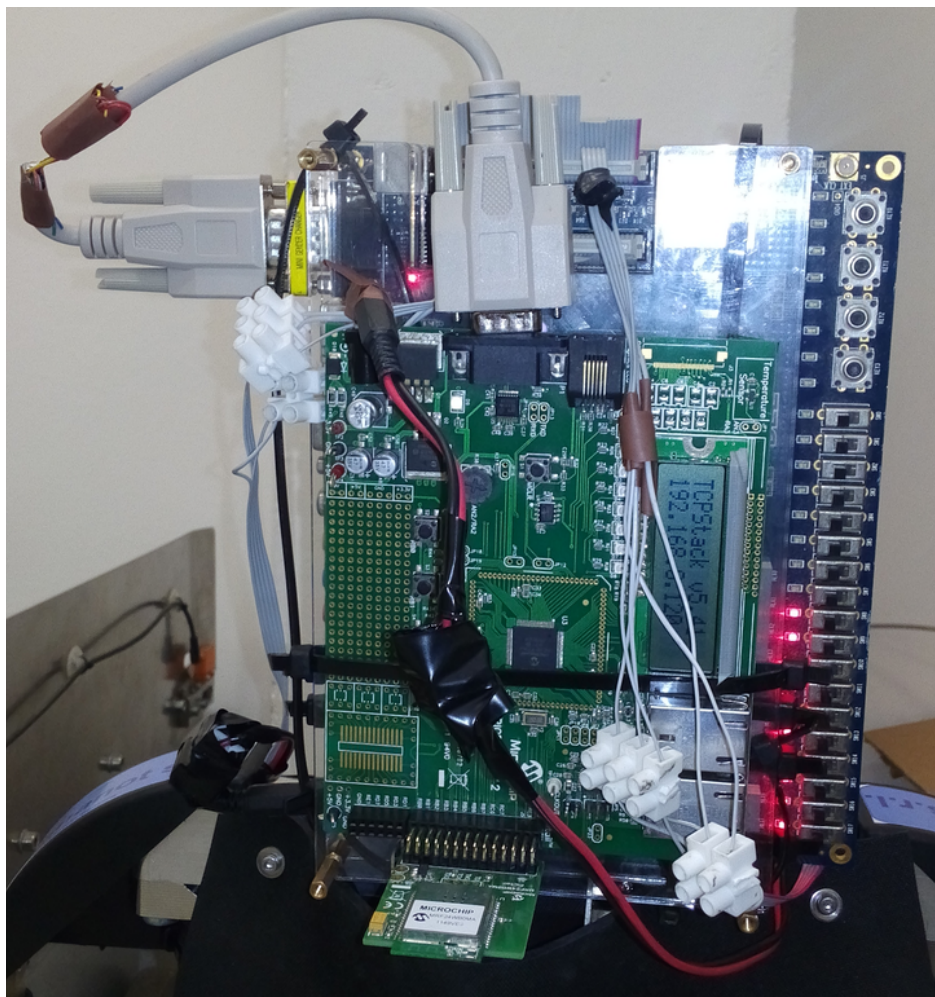


Figure 6: Wires and connectors of Rollo.



Figure 7: Wooden stabilization pieces after cutting and drilling holes used to make the Rollo more rigid.

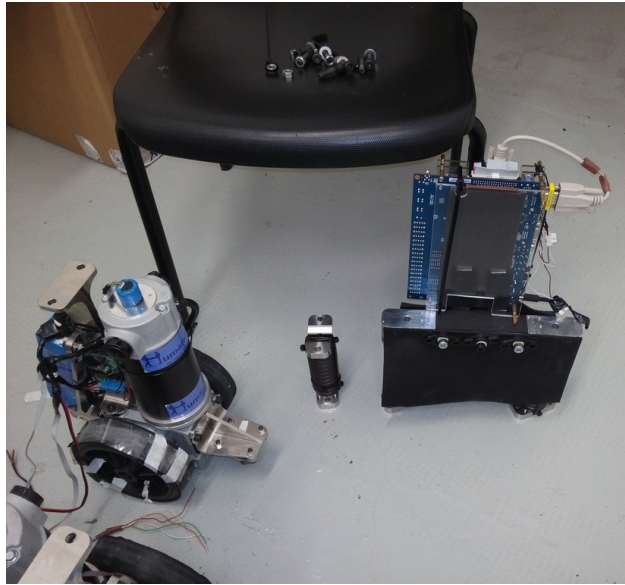


Figure 8: Rollo disassembled.

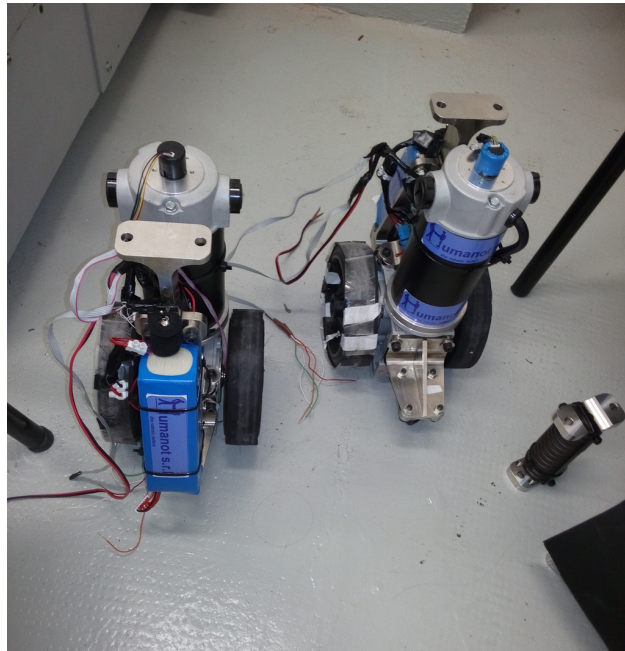


Figure 9: Lower legs of Rollo.

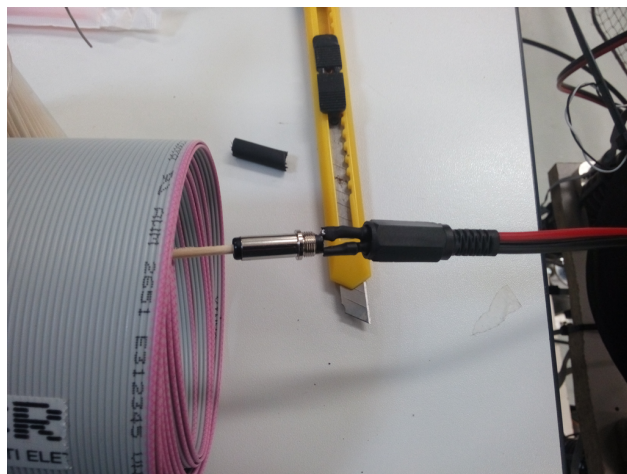


Figure 10: Preparation of power connectors for the microcontroller boards with help of thermoshrink.

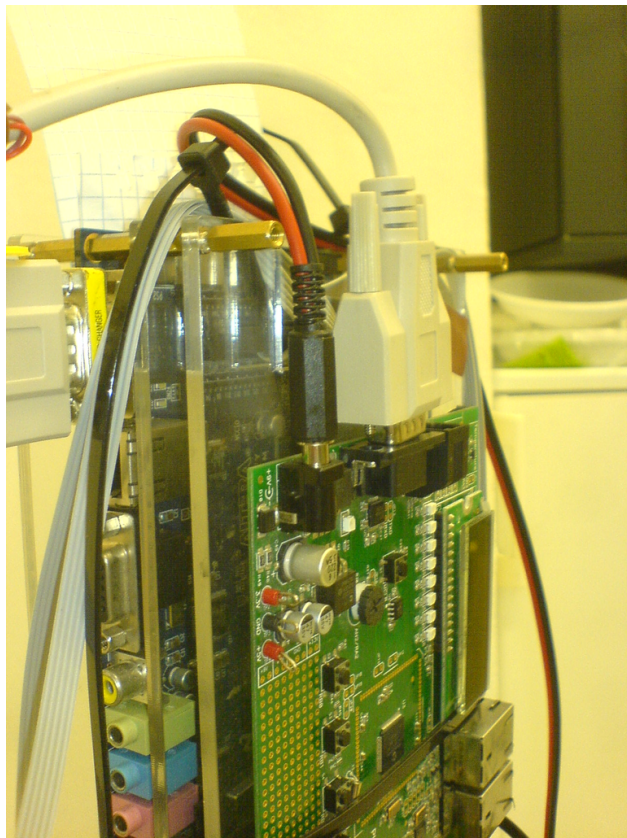


Figure 11: Power connector in final state.

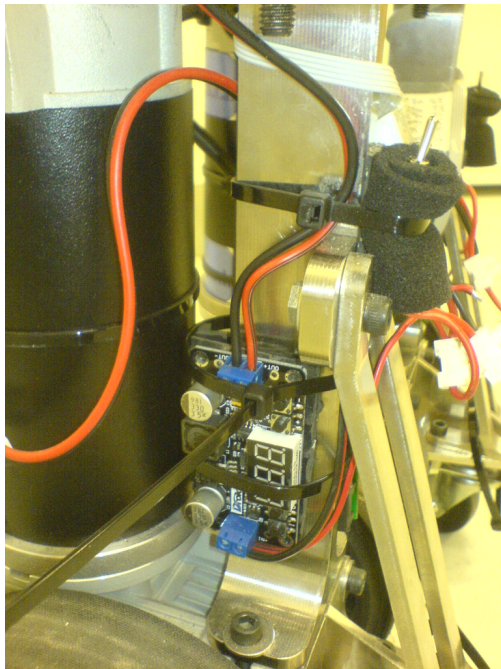


Figure 12: Voltage regulator with new power cables. The cable tie was used to secure the damaged power connector case, which was of very poor quality.



Figure 13: Control cable for the motor controller with a connector table for easy access.

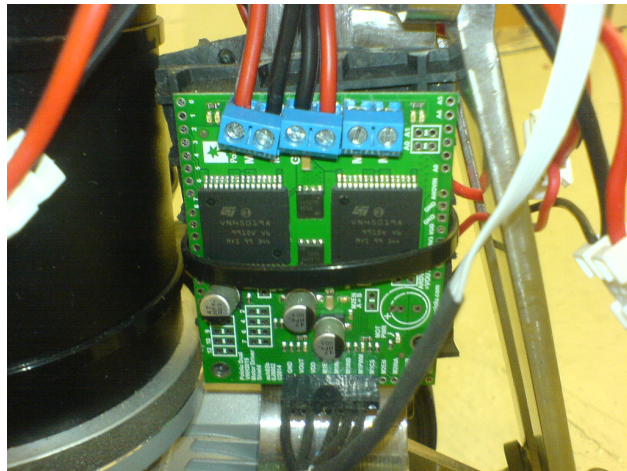


Figure 14: Motor controller using proper control signal connectors with high quality isolation and new power cables.



Figure 15: Power and control signal cables secured using cable ties. The encoders were connected using professional soldering technique and isolated properly.

At one point during the work with Rollo one of the power connectors caused a short circuit, which damaged the DROK voltage regulator's semiconductor integrated circuit LM2596 seen in figure 12. After this incident the decision was made to replace all power connections with new power cables with higher and only one diameter. Also all control signal cables have been replaced and secured with cleaned up cable ties as seen through figures 10 ÷ 16. Only the VGA socket cable connecting both microcontroller boards has not been replaced, however it's connections have also been improved.

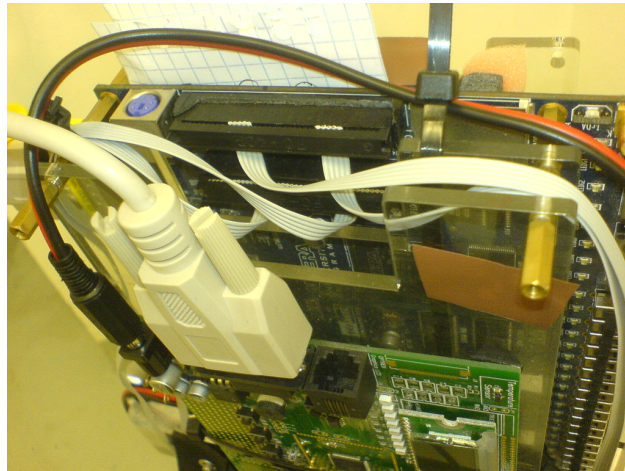


Figure 16: Encoder and motor controller connections to the microcontroller board using IDE40 cables.

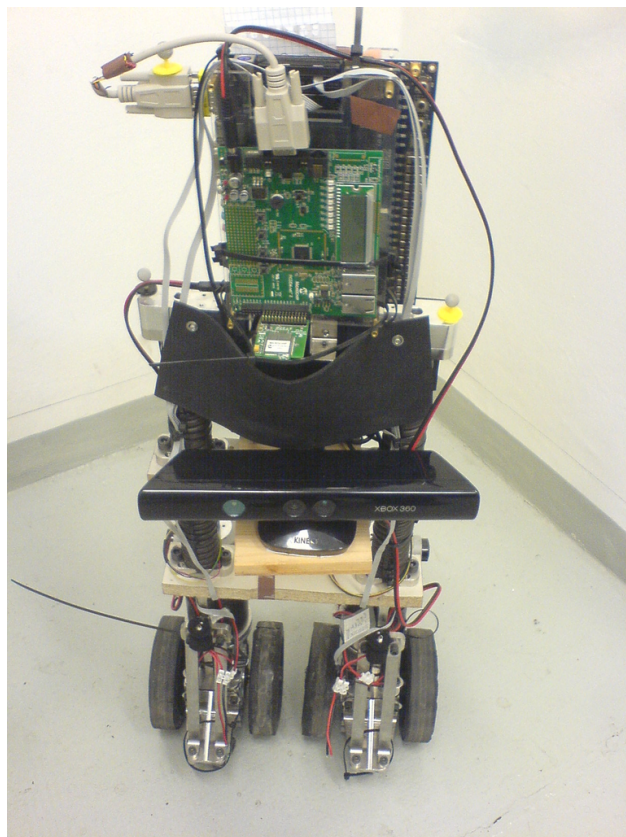


Figure 17: Final state of Rollo after improvements. Additional hardware in form of Kinect andd RaspberryPi have been added for another project.

The final state after mechanical and electrical improvements can be seen in image in figure 17. The introduced improvements provided a safe and disturbance-free operation not only for this project. Also the capability of reading the encoders has been enabled through a complete rewiring and clean-up of signal cables.

Simulation and testing

Simulation of extended Kalman filter

EKF algorithm was first simulated in Matlab using recorded data from Rollo's test runs. Measurement logs were collected for the robot's straight line test runs and initial value of measurement was set as the initial state estimate. EKF update was performed using this initial state estimate, control input for the given log and measurement for the log.

Figure 18 shows the results of EKF based on one of a log file. $x_{state}[1]$ and $x_{state}[2]$ represent position of robot in x and y coordinates in meters respectively. $x_{state}[3]$ represents orientation Θ of the robot in radians. The blue lines show the state estimates updates with EKF, while the red lines represent the measurement, which is the actual state.

It can be observed from the plots that the EKF based state estimates are influenced by measurement and are able to converge to the varying values of measurement.

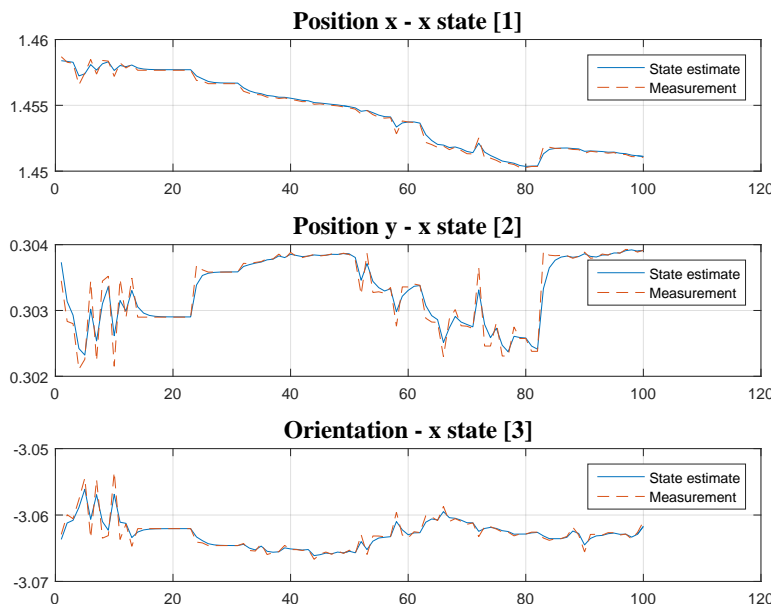


Figure 18: Results of EKF simulation based on a log file.

Figure 19 shows the results of EKF update for longer iterations to verify the stability of EKF. If original EKF equations are directly used with the system, the state estimate and state covariance matrix starts to diverge after sometime, as discussed in section Divergence of state covariance matrix $\Sigma_{k|k}$. This figure shows result of performing Cholesky decomposition for measurement update.

Testing of extended Kalman filter

Test setup

In order to conduct the tests both battery packs were fully charged and five infrared markers were placed on Rollo at different points, creating an asymmetrical structure, so that it could be reliably tracked by the motion capture system.

The motion capture system itself, was calibrated so that the x -axis and y -axis for localization were defined according to Cartesian coordinate system. The Robot was placed in the test area with its orientation aligned to x -axis, ergo pointing eastwards from the operational station position, and then defined as a rigid

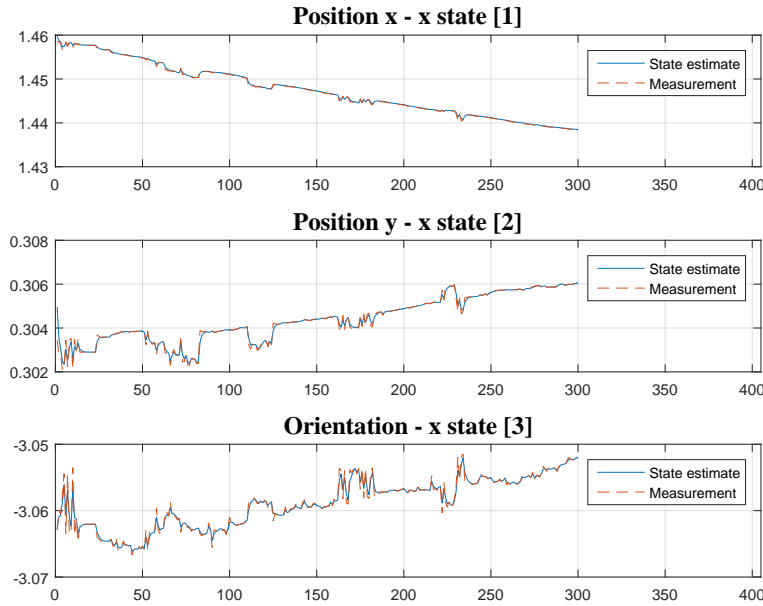


Figure 19: Results of EKF simulation based on a log file for longer iterations to verify stability.

body in the motion capture system. This ensured that the orientation of the robot was 0 radians when it was aligned to x -axis similar to the developed odometry model.

The complete software package that received localization from the motion capture system, controlled Rollo, processed data to implement EKF and visualization was developed within the ROS framework as described in Robot Operating System (ROS). Rollo was manually controlled using the keyboard and communication with Rollo was done at 10Hz. The preprocessor node, responsible for gathering and processing of measurement data, was updated 25 Hz. Hence, the EKF update was also performed approximately at a rate of 25 Hz. Testing sessions during development showed, that the EKF node could be easily run at a frequency rate of 10 Hz and still produce reasonable results, which when visualized were barely

Unfortunately, the encoder feedback was unavailable for the test, however the communication node was reprogrammed to send certain angular velocities for the wheels at a given command. The complete range of velocities was not covered, only the command values shown in the table 1 were tested. This is due to anticipation of more precise results using lower half of velocity range, which resulted in reprogramming of Rollo low-level software itself to accommodate this request.

In the start of each test run, the robot position and orientation read from the motion capture system was used as the initial state estimate. Initial state covariance matrix was set as identity matrix.

State prediction using the odometry based model alone was also studied for comparison with EKF based model. However, in the absence of encoder data this model was very crude. Moreover, the testing floor was uneven and had visible irregularities, which introduced non systematic errors that are not modelled in the odometry.

Initial state for the odometry model was taken as the same state for the EKF based model. The logs were collected sometime after the test was conducted and analyzed. This was due to lag in the system. However, the videos of online visualization for the tests were recorded from the very start of the run. There were several technical difficulties including problems with networking that obstructed optimal testing conditions. Rollo on multiple occasions lost signal to the provided wireless router and continued running with last received command. This has also been a factor behind the decision to implement emergency procedure into the communication node, even though this problem persists, because of the provided hardware and low-level

software of Rollo.

There were also problems with Optitrack Motion Capture system that had difficulties providing clear images of the scene at reasonable frame rates of 90 *fps* relative to system's maximum of 120 *fps*, using the grayscale reference video mode.

Testing variables

Rollo was tested with different process covariance matrix Q and measurement covariance matrix R values to analyse EKF performance. The two matrices and their properties are described in detail in System and measurements model, Measurement model with noise and Divergence of state covariance matrix $\Sigma_{k|k}$.

For process noise covariance matrix, it was assumed that the noise sources were independent for the three states, position in x and y coordinates and the orientation Θ , and the noise variances for all three states were assumed to be equal and constant. Assigning the standard deviation for all states as q , the Q matrix can be written as shown in (51).

$$Q_k = \begin{bmatrix} q^2 & 0 & 0 \\ 0 & q^2 & 0 \\ 0 & 0 & q^2 \end{bmatrix} \quad (51)$$

Similarly for measurement noise covariance matrix the same assumption has been made. Assigning the standard deviation for the all states as r , the R matrix can be written as shown in (52).

$$R_k = \begin{bmatrix} r^2 & 0 & 0 \\ 0 & r^2 & 0 \\ 0 & 0 & r^2 \end{bmatrix} \quad (52)$$

Table 2: Predetermined wheels angular velocity based on test logs for given forward command.

q	r
0.1	0.1
0.1	1.0
0.1	10.0
1.0	10.0
10.0	10.0
100.0	10.0
8.0	32.0

Table 2 enlists the combinations of q and r that were tested. The EKF update rate was at 10 *Hz* for those particular test runs. For every test the initial state estimate was reassigned and the EKF node was restarted, so that the odometry model could be reinitialized to the same position as EKF estimate.

Test results and analysis

During online testing the localization was studied using the visualization node. A snapshot of the real time visualization is shown in figure 20.

Logs were generated for offline and in-depth analysis of the system. ROS provides the capability to rerun the tests from recorded logs and evaluate the performance of nodes again based on the same data. Several Bash scripts have been written specifically for the purpose of easier repetition of recording and replaying of acquired log data as described in the GitHub repository files list.

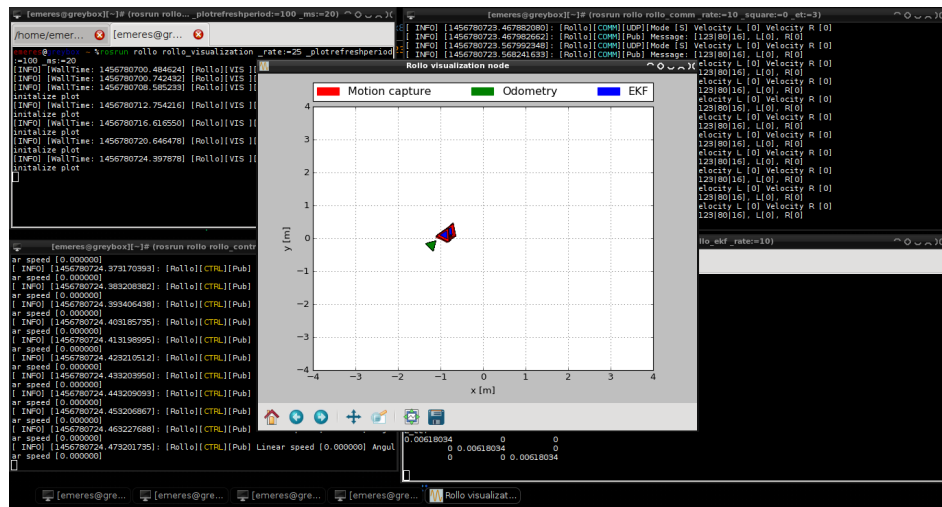


Figure 20: Real time visualization: localization of the robot based on EKF, odometry alone and the measurement.

For every test run two different plots were generated. One showed position of the robot computed according to odometry, EKF and motion capture system and the second plot displayed position and orientation of the robot with respect to time. Chosen plots of the conducted test runs are shown and described in this section.

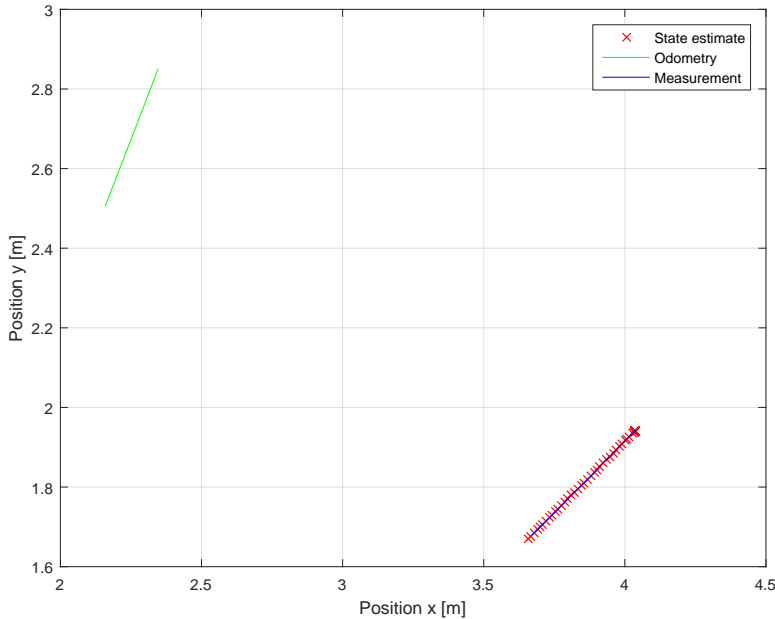


Figure 21: Test 1, velocity command 19% for both left and right wheels, $q = 0.1$, $r = 0.1$.

Initial tests were conducted for $q = 0.1$ and $r = 0.1$. Figures 21 and 22 show a straight line run for 19% velocity command. It can be observed from the plot that the state estimate is almost superimposed on measurement line at each computation point. This proves that the implemented EKF is capable of very accurate state estimation. Odometry even though intuitively showing completely incorrect results by drifting

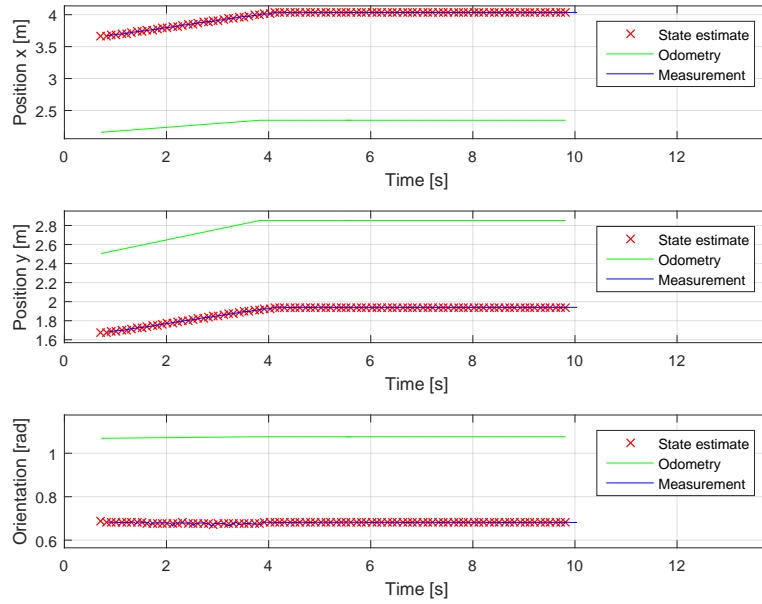


Figure 22: Test 1, velocity command 19% for both left and right wheels, $q = 0.1$, $r = 0.1$. Figure shows all three states with respect to time.

far from actual position of the robot with time, shows the same character of Rollo's movement. Since this was only crudely modelled without encoders feedback, no efforts were made to improve it. The reason for symmetrically opposite movement was an error in communication node, where velocities estimates for left and right wheels were switched. Also here the EKF node was not restarted properly, resulting in odometry model having a different initial position and orientation.

The initial values of q and r involved in EKF yielded respectable performance. Further tests were performed by adding more noise to the measurement model using a larger r .

By taking $q = 0.1$ and $r = 1.0$, the tracking ability of EKF was reduced. Figures 23 and 24 show a straight line run for 12% velocity command. It can be observed that the state estimate was close to the measurement line, but was unable to reach it and remained at a varying offset to the measurement.

Further noise was added to the measurement model by setting $q = 0.1$ and keeping $r = 10.0$. Figures 25 and 26 show plots of a counter clockwise rotation for 12% left velocity command and 19% right velocity command. State estimate visibly drifted from the actual position. Therefore, with the increase in measurement noise, the weight of measurement data is lower in the Kalman filter. Further tests were conducted with r kept constant at value 10. Also worth noting are the slips of Rollo's wheels visible by jumps in the measurement data. As already mentioned, the laboratory ground was uneven and irregular introducing random errors, especially during rotations of Rollo.

Figures 27 and 28 show another counter clockwise rotation at 12% left velocity command and 19% right velocity command for $q = 1.0$ and $r = 10.0$. In this scenario the EKF response has widely improved. By increasing the value of q the uncertainty in process model was also increased. In comparison to previous test, the measurement had more significance. However, an error between the EKF based state estimate and the measurement can still be seen.

Further noise was added to the process model by increasing q to the value 10. Figures 29 and 30 portray a counter clockwise rotation at 12% left velocity command and 19% right velocity command for $q = 10.0$ and $r = 10.0$. It can be observed that the EKF was again able to track the localisation of the robot very well. The performance is comparable to results seen in test 1, when the values for q and r were equal at value 0.1.

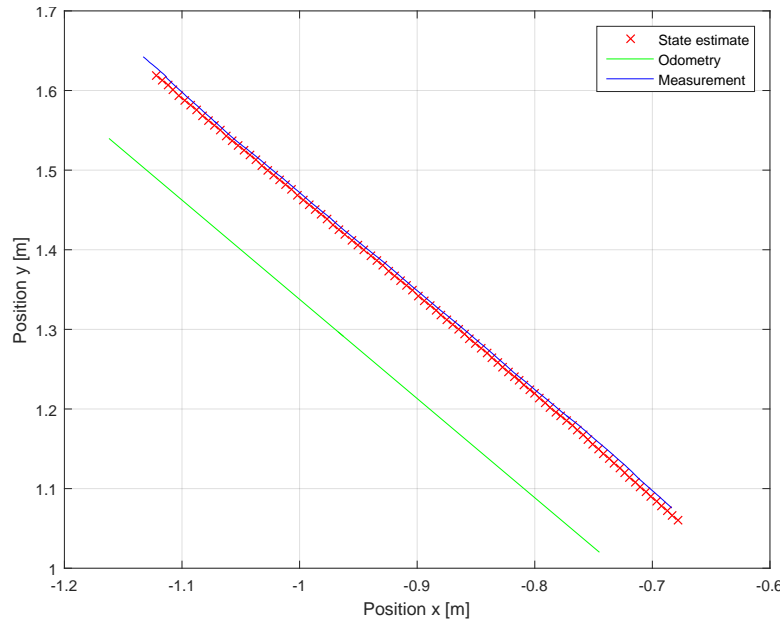


Figure 23: Test 2, velocity command 12% for both left and right wheels, $q = 0.1$, $r = 1.0$.

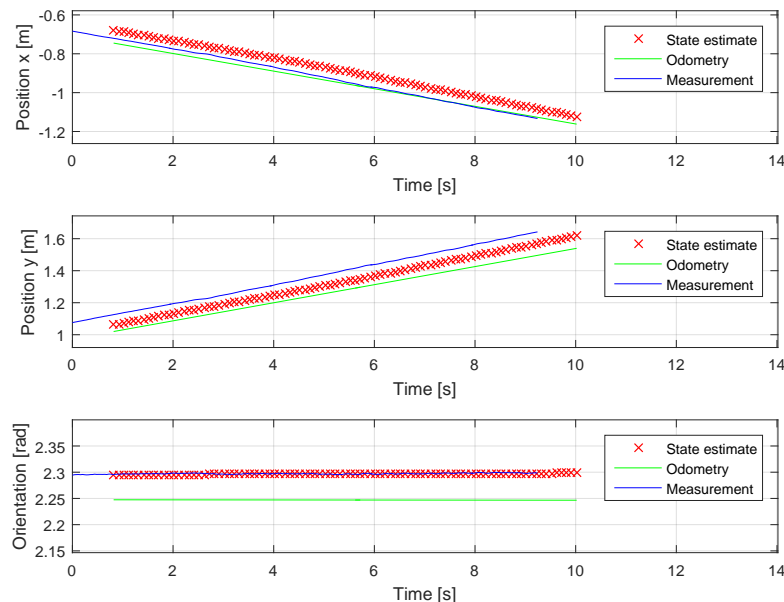


Figure 24: Test 2, velocity command 12% for both left and right wheels, $q = 0.1$, $r = 1.0$. Figure shows all three states with respect to time.

Thus, it can be understood that the relative ratio between Q and R matrices determines the performance of EKF, not the absolute values of Q and R alone.

In figures 31 and 32 a clockwise rotation at 19% left velocity command and 12% right velocity command for $q = 100.0$ and $r = 10.0$ was plotted. Again, by increasing the value of q more noise was added to the process model and therefore the measurement gained more influence on the estimates in the Kalman filter

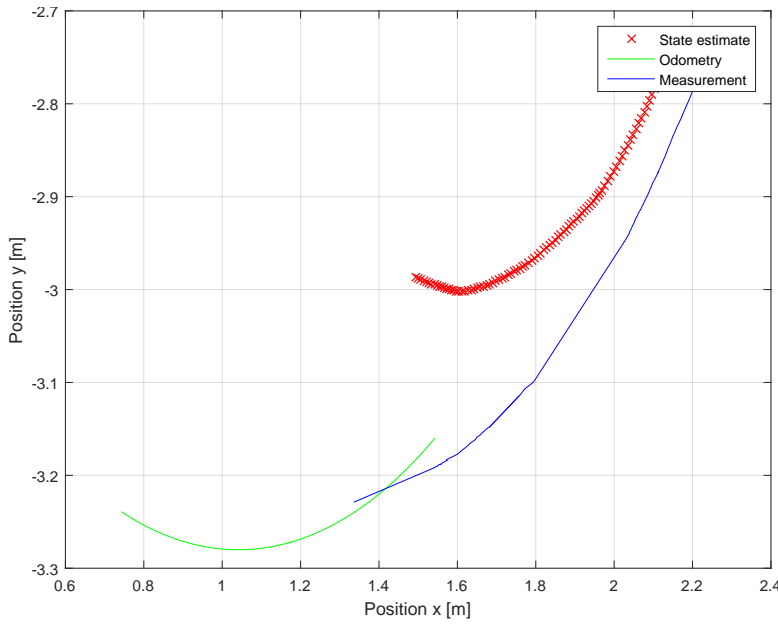


Figure 25: Test 3, velocity command 12% for left wheel and 19% for right wheel, $q = 0.1$, $r = 10$.

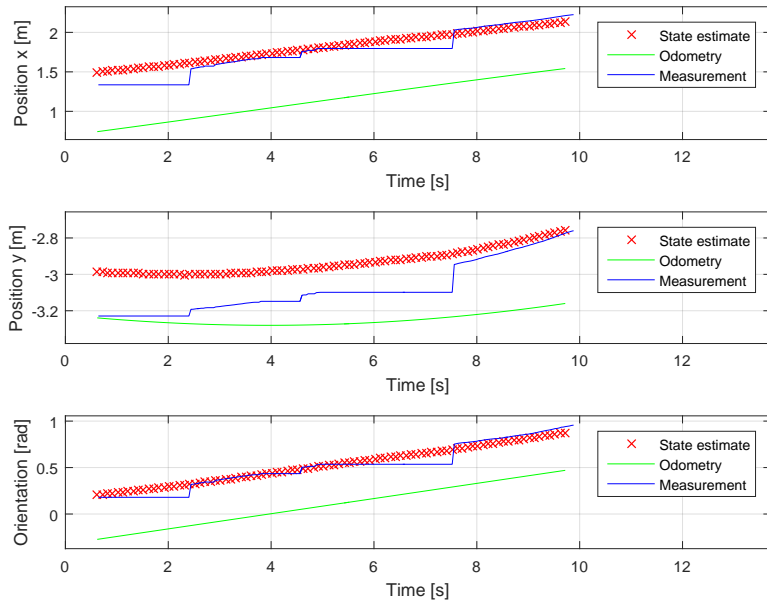


Figure 26: Test 3, velocity command 12% for left wheel and 19% for right wheel, $q = 0.1$, $r = 10$. Figure shows all three states with respect to time.

model. It can be clearly observed that EKF is easily able to localize the robot very accurately. Measurement sensors from the motion capture system provide, after a proper calibration, very accurate readings of Rollo's localization.

Final test was performed with values $q = 8.0$ and $r = 32.0$. Figures 33 and 34 show plots of a counter clockwise rotation at 12% left velocity command and 19% right velocity command. Since r was greater than

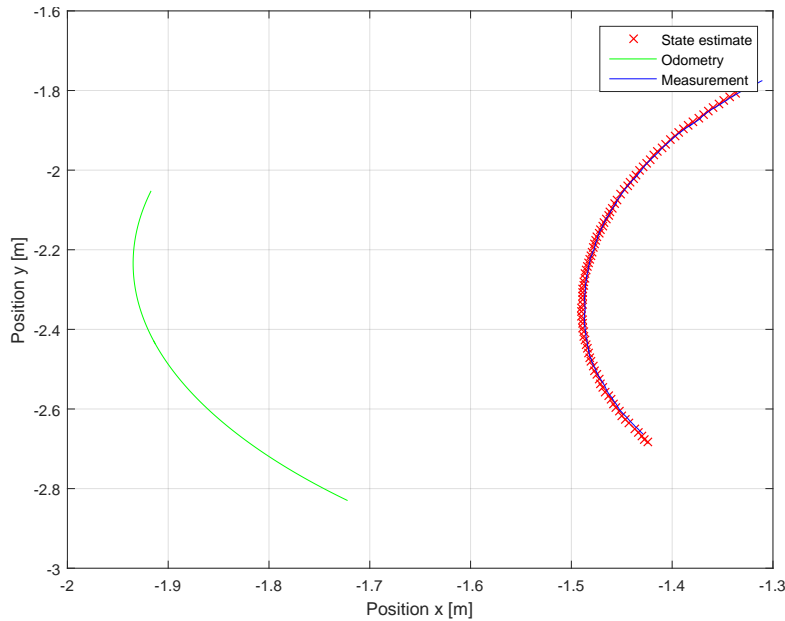


Figure 27: Test 4, velocity command 19% for left wheel and 12% for right wheel, $q = 1.0$, $r = 10$.

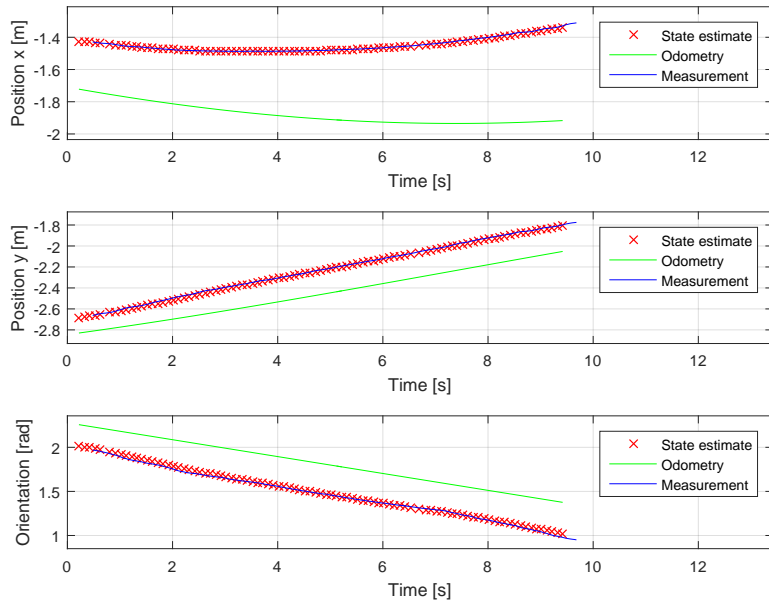


Figure 28: Test 4, velocity command 19% for left wheel and 12% for right wheel, $q = 1.0$, $r = 10$. Figure shows all three states with respect to time.

q , the measurement model has had a lower impact on the Kalman filter as compared to the process model. It can be observed from the plots that the EKF was unable to localize the robot accurately and state estimate has visibly drifted from the actual position of Rollo, especially during the curve.

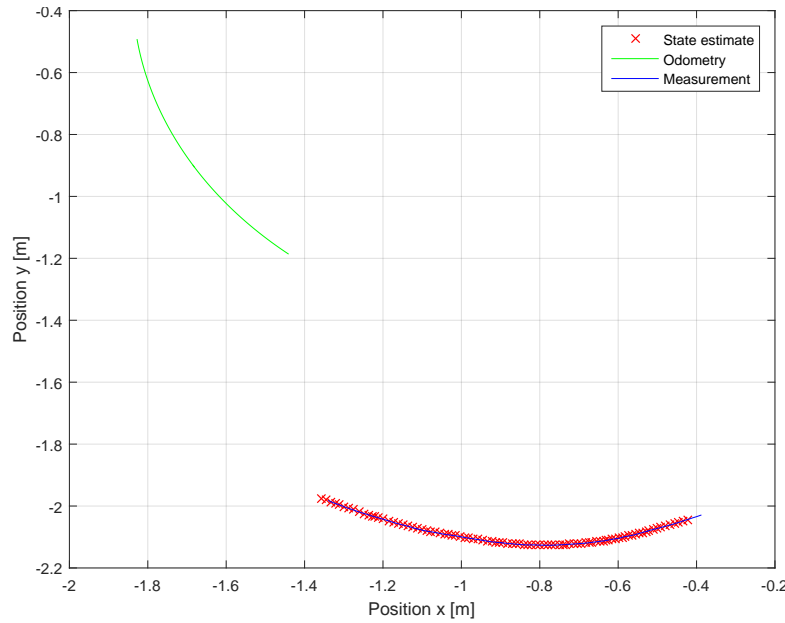


Figure 29: Test 5, velocity command 12% for left wheel and 19% for right wheel, $q = 10$, $r = 10$.

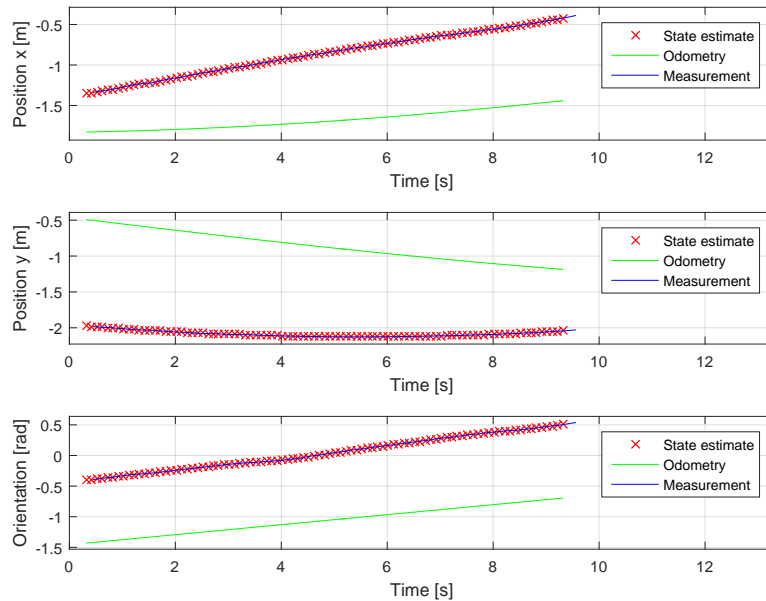


Figure 30: Test 5, velocity command 12% for left wheel and 19% for right wheel, $q = 10$, $r = 10$. Figure shows all three states with respect to time.

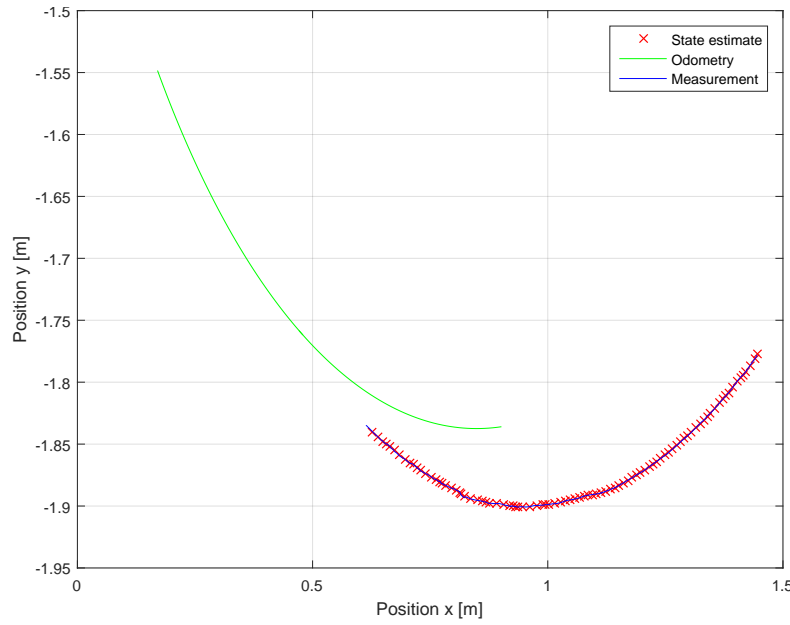


Figure 31: Test 6, velocity command 19% for left wheel and 12% for right wheel, $q = 100$, $r = 10$.

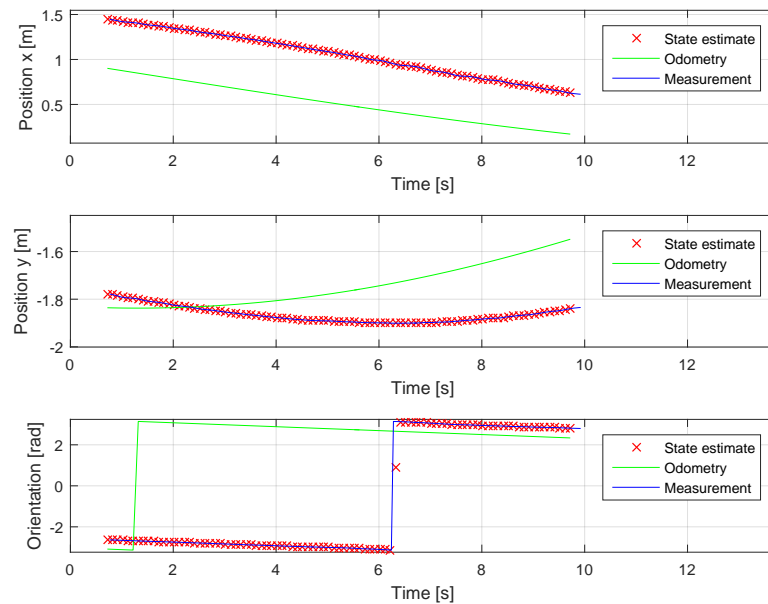


Figure 32: Test 6, velocity command 19% for left wheel and 12% for right wheel, $q = 100$, $r = 10$. Figure shows all three states with respect to time.

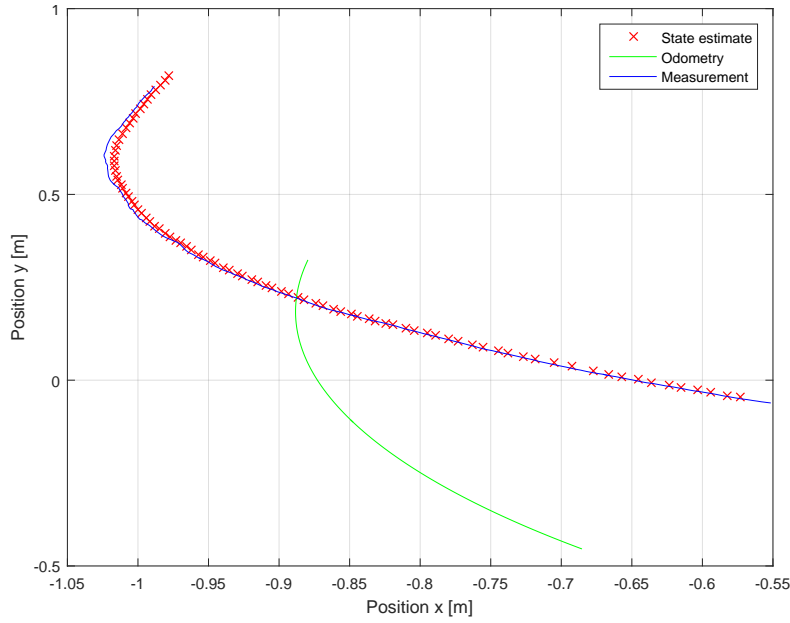


Figure 33: Test 7, velocity command 12% for left wheel and 19% for right wheel, $q = 8, r = 32$.

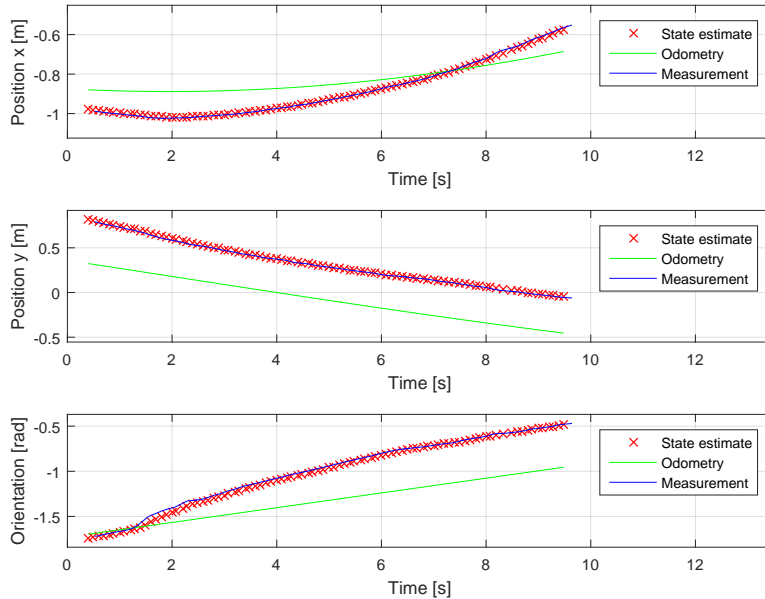


Figure 34: Test 8, velocity command 12% for left wheel and 19% for right wheel, $q = 8, r = 32$. Figure shows all three states with respect to time.

Conclusions

Localization in technology is the estimation of position and state of a system in the world frame of reference by making use of limited information. Localization has been one of the primary challenges in robotics in the field of mobile robots. It is very common in mobile robots to use odometry and inertial measurement unit (IMU) as relative position sensors and GPS as absolute position sensor to estimate state of the robot. Extended Kalman filter is a widely used filtering technique in estimating the localization of a robot that processes feedback from two or more sensors.

The presented project starts with preparing the odometry based physical model of Rollo, showing it's advantages and disadvantages with respect to the localization problem. Furthermore errors associated with odometry, divided into systematic and non systematic, were presented along with the UMBmark based square test technique to determine dominant odometry errors.

Next the preparation of the system and measurement models was conducted and the equations for the implementation of Kalman filter and then extended Kalman filter were defined. EKF was first simulated and verified in Matlab. The final tests were conducted on Rollo and the performance of extended Kalman filter was analysed by varying process covariance matrix Q and measurement covariance matrix R . Given appropriate ratio between the covariances the implemented EKF performs satisfactory and solves the problem of localization of Rollo.

Additional improvements like the square test and Cholesky decomposition have been implemented into the developed software, along with various other aspects, like a standalone odometry model written in Python. Also mechanical and electrical improvements have been performed on Rollo as described in section Mechanical and electrical improvements.

For future work, it is proposed to first implement encoders feedback in the system and validate the EKF with working odometry. This would also require expanding current ROS nodes, especially the communication node. Even though the encoders feedback is currently unavailable in Rollo, the modelling of the system and software was designed for a swift and easy transition to odometry feedback. Furthermore, another sensor should be introduced in the system, since the motion capture system will most probably be unavailable in real life applications.

In regards to the mechanical system of the robot, it is recommended that a different material for the wheels should be used to improve traction and reduce skidding of the robot. The wheels of the robot also need to be properly aligned so that the odometry errors are reduced.